Combustion and Flame 162 (2015) 4566–4585

Contents lists available at ScienceDirect

Combustion and Flame

journal homepage: www.elsevier.com/locate/combustflame

Direct numerical simulations of ignition of a lean *n*-heptane/air mixture with temperature and composition inhomogeneities relevant to HCCI and SCCI combustion

Minh Bau Luong[a], Gwang Hyeon Yu[a], Tianfeng Lu[b], Suk Ho Chung[c], Chun Sang Yoo[a,d,*]

[a] Department of Mechanical Engineering, Ulsan National Institute of Science and Technology, Ulsan 689-798, Republic of Korea
[b] Department of Mechanical Engineering, University of Connecticut, Storrs, CT 06269, USA
[c] Clean Combustion Research Center, King Abdullah University of Science and Technology, Thuwal, Saudi Arabia
[d] School of Mechanical and Nuclear Engineering, Ulsan National Institute of Science and Technology, Ulsan 689-798, Republic of Korea

ARTICLE INFO

Article history:
Received 13 March 2015
Revised 16 September 2015
Accepted 16 September 2015
Available online 22 October 2015

Keywords:
Direct numerical simulation (DNS)
Homogeneous-charge compression ignition (HCCI)
Stratified-charge compression ignition (SCCI)
Negative-temperature coefficient (NTC)
Chemical explosive mode analysis (CEMA)

ABSTRACT

The effects of temperature and composition stratifications on the ignition of a lean *n*-heptane/air mixture at three initial mean temperatures under elevated pressure are investigated using direct numerical simulations (DNSs) with a 58-species reduced mechanism. Two-dimensional DNSs are performed by varying several key parameters: initial mean temperature, T_0, and the variance of temperature and equivalence ratio (T'' and ϕ'') with different $T-\phi$ correlations. It is found that for cases with ϕ'' only, the overall combustion occurs more quickly and the mean heat release rate (HRR) increases more slowly with increasing ϕ'' regardless of T_0. For cases with T'' only, however, the overall combustion is retarded/advanced in time with increasing T'' for low/high T_0 relative to the negative-temperature coefficient (NTC) regime resulting from a longer/shorter overall ignition delay of the mixture. For cases with uncorrelated $T-\phi$ fields, the mean HRR is more distributed over time compared to the corresponding cases with T'' or ϕ'' only. For negatively-correlated cases, however, the temporal evolution of the overall combustion exhibits quite non-monotonic behavior with increasing T'' and ϕ'' depending on T_0. All of these characteristics are found to be primarily related to the 0-D ignition delays of initial mixtures, the relative timescales between 0-D ignition delay and turbulence, and the dominance of the deflagration mode during the ignition. These results suggest that an appropriate combination of T'' and ϕ'' together with a well-prepared $T-\phi$ distribution can alleviate an excessive pressure-rise rate (PRR) and control ignition-timing in homogeneous charge compression-ignition (HCCI) combustion. In addition, critical species and reactions for the ignition of *n*-heptane/air mixture through the whole ignition process are estimated by comparing the temporal evolution of the mean mass fractions of important species with the overall reaction pathways of *n*-heptane oxidation mechanism. The chemical explosive mode analysis (CEMA) verifies the important species and reactions for the ignition at different locations and times by evaluating the explosive index (EI) of species and the participation index (PI) of reactions.

1. Introduction

Among many low-temperature combustion (LTC) engines, homogeneous-charge compression ignition (HCCI) engines have emerged as one of the most probable alternatives to conventional gasoline and diesel engines. HCCI engines are designed to operate under low-temperature conditions by utilizing lean, highly-diluted, well-mixed fuel/air charge with elevated compression ratios. Therefore, they can provide high diesel-like thermal efficiency and avoid excessive NO*x* and particulate emissions without the help of high-price after-treatment devices.

Despite their advantages over the conventional internal combustion (IC) engines, however, the development of practical HCCI engines remains challenging mainly due to two unresolved issues: an excessive pressure-rise rate (PRR) which may lead to pressure ringing and even to engine knocking, and unprecise ignition-timing control. Fuel/air mixture in HCCI engines is usually well-premixed, and auto-ignited by the compression heating by the piston motion. Therefore, overall combustion in an HCCI engine cylinder is generally believed to occur by simultaneous auto-ignition, which may lead to an excessive PRR, ultimately damaging the engine block. In addition, the auto-ignition in the HCCI engine is primarily determined by the in-cylinder conditions such as overall pressure, temperature, equivalence ratio,

* Corresponding author at: School of Mechanical and Nuclear Engineering, Ulsan National Institute of Science and Technology, Ulsan 689-798, Republic of Korea. Fax: +82 52 217 2409.
E-mail address: csyoo@unist.ac.kr, withspring@gmail.com (C.S. Yoo).

http://dx.doi.org/10.1016/j.combustflame.2015.09.015
0010-2180/

and their fluctuations and hence, the precise control of ignition timing of HCCI combustion should be achieved by a well-designed mixture composition and the amount of exhaust gas recirculation (EGR) [1–4].

One of the most effective methods to overcome the excessive PRR under high-load operating conditions in the HCCI engines is to generate a sequential ignition event by using in-cylinder mixture inhomogeneities. Numerous experimental and numerical studies of HCCI combustion have shown that thermal and compositional stratifications of the in-cylinder fuel/air mixture can provide a smooth combustion process under high-load conditions by changing the combustion mode from spontaneous ignition into a mixed combustion mode of spontaneous ignition and deflagration [1–21].

In many previous direct numerical simulation (DNS) studies [7–13], it was found that thermal stratification may effectively control ignition timing and smooth out the excessive PRR regardless of the in-cylinder mean temperature near the top dead center (TDC). However, the management and utilization of the in-cylinder thermal stratification is not straightforward and as such, it still remains challenging to apply thermal stratification to the development of prototype HCCI engines [1,14,15]. Instead, stratified-charge compression ignition (SCCI) combustion, which introduces a certain degree of fuel inhomogeneities in fuel/air mixture, has been devised as another promising remedy for the problems in HCCI combustion. In general, fuel inhomogeneities may induce a sequential ignition event, resulting in a prolonged combustion process under certain conditions [12,14,16,17].

In practice, the fuel stratification for SCCI combustion can be achieved by multiple high-pressure injectors with precisely-controlled injection timing [3,4,16]. In two-stage injection, for instance, the main portion of fuel is first supplied during the intake stroke using a port fuel injector to generate relatively-homogeneous fuel/air mixture [16] and additional fuel (up to 20% of total fuel volume) is then directly injected during the late compression stroke or near the TDC to introduce a certain degree of fuel concentration stratification [4]. Typically, a higher degree of in-cylinder fuel stratification can be obtained by increasing the fraction of directly-injected fuel and/or retarding direct injection timing [22]. Due to the practical importance of SCCI combustion, many fundamental studies of SCCI combustion with different fuels have been performed [1,14–33].

Several DNS studies of ignition of thermally and compositionally stratified hydrocarbon/air mixtures have been carried out [12,34–36]. Mittal et al. [34] investigated the ignition characteristics of *n*-heptane/air mixture with uncorrelated thermal and compositional stratifications under HCCI and diesel combustion limits to develop a generalized multi-regime representative interactive flamelet (RIF) model. Although several different levels of fluctuations were adopted for two-dimensional (2-D) DNSs, only uncorrelated temperature and composition fields were considered to validate the RIF model and as such, the discussion was also limited to the model validation. Luong et al. [12] elucidated the ignition characteristics of a lean biodiesel/air mixture with both temperature and composition inhomogeneities under HCCI conditions by using 2-D DNSs. It was found that a harmonious combination of composition and temperature fluctuations can prevent an excessive heat release rate (HRR) and control the ignition timing more effectively than temperature fluctuation only. However, the ignition of a lean biodiesl/air mixture under HCCI conditions exhibit relatively-weak NTC behavior and as such, the effects of the strong NTC behavior of fuel/air mixture on the HCCI combustion were not fully appreciated.

Recently, Talei and Hawkes [35] investigated the effects of negatively-correlated temperature and composition stratifications on the ignition of *n*-heptane/air mixture with different levels of mixture stratification. They found that negatively-correlated fields always advance the overall combustion compared to 0-D ignition regardless the degree of the stratifications. However, their parametric study was limited to only a few cases with negatively-correlated temperature and composition fields within the NTC regime. More recently, Bansal et al. [36] examined the characteristics of auto-ignition of stratified dimethyl ether (DME)/air mixture using 2-D and 3-D DNSs. It was found that compression heating can alter the overall HCCI combustion by lowering temperature gradient of the initial field. It was also found that the overall combustion of negatively-correlated case occurs primarily by spontaneous ignition but that of uncorrelated case leads to conventional premixed deflagrations. In most studies, however, the effects of temperature and composition stratification together with their correlation on HCCI combustion were investigated fragmentarily and as such, it is not simple to generally understand each effect on HCCI/SCCI combustion.

Therefore, the objective of the present study is twofold: (1) to elucidate the effects of initial mean temperature in conjunction with both thermal and compositional stratifications on the ignition characteristics of realistic hydrocarbon fuel/air mixture under HCCI conditions in a comprehensive manner by performing 2-D DNSs and (2) to provide a better understanding of its temporal and spatial ignition characteristics with the chemical explosive mode analysis (CEMA). In this study, *n*-heptane is adopted as a hydrocarbon fuel, which exhibits a strong NTC behavior under HCCI conditions. Note that *n*-heptane has been widely used as a viable surrogate in both experimental and numerical studies to elucidate the ignition characteristics of the HCCI combustion [9].

2. Numerical method and initial conditions

For the present DNSs, Sandia DNS code, S3D, was used to solve the compressible Navier–Stokes, species continuity, and total energy equations. S3D was linked with CHEMKIN and TRANSPORT software libraries [37,38] to evaluate thermodynamic and mixture-averaged transport properties. A fourth-order explicit Runge–Kutta method [39] and an eighth-order central differencing scheme [40] were employed for time integration and spatial discretization, respectively. A tenth-order filter was also applied to eliminate any spurious high-frequency fluctuations in the solution. For a detailed description of the numerical methods, readers are referred to [41]. Periodic boundary conditions were imposed in all directions of the computational domain and as such, the ignition of an *n*-heptane/air mixture occurs at a constant volume.

As in [9], the 58-species *n*-heptane/air reduced mechanism was adopted. Although the 58-species reduced mechanism is significantly simplified from the detailed mechanism, it still shows a good agreement with the detailed mechanism and experiments in terms of ignition delays, flame propagation speeds, and extinction residence times under a wide range of initial temperature, equivalence ratio, and pressure conditions. The stiffness removal technique was adopted to remove any chemical timescales shorter than 10 ns [42]. This technique has been extensively validated through numerous homogeneous and 1-D ignition test cases, and 2-D DNS applications [9–13,42].

For all DNSs, the initial mean equivalence ratio, ϕ_0, and initial uniform pressure, p_0, are 0.45 and 40 atm, respectively. Several parametric studies were performed to elucidate the effects of the initial mean temperatures, T_0, with the variances of temperature, T', and/or equivalence ratio, ϕ', on the ignition of a *n*-heptane/air mixture under HCCI conditions. Total 23 2-D DNSs were carried out by varying three key parameters: (1) T_0 of 805, 933, and 1025 K, (2) T' of 0, 15, and 60 K, and (3) ϕ' of 0, 0.05, and 0.10. Three initial mean temperatures with identical 0-D ignition delay, τ^0_{ig}, of 1.5 ms were selected. Details of the physical parameters for the 23 DNS cases are listed in Table 1.

Note that Dec and Hwang [5] found that thermal stratification level naturally occurring in an HCCI engine is approximately $T' = 13.3$ K which corresponds to $T' = 15$ K in the present study. In

Table 1
Physical parameters of Cases 1–23. BL represents a baseline case with either T' only or ϕ' only. UC and NC represent uncorrelated $T-\phi$ and negatively-correlated $T-\phi$ distribution, respectively.

Case	Type	T_0 (K)	T' (K)	ϕ_0	ϕ'	l_e (mm)	l_{Te} (mm)	$l_{\phi e}$ (mm)	u' (m/s)	τ_t (ms)	τ_{ig}^0 (ms)
1	BL	805	15	0.45	–	1.25	1.25	–	0.83	1.5	1.5
2	BL	805	60	0.45	–	1.25	1.25	–	0.83	1.5	1.5
3	BL	805	–	0.45	0.05	1.25	–	1.25	0.83	1.5	1.5
4	BL	805	–	0.45	0.10	1.25	–	1.25	0.83	1.5	1.5
5	BL	933	15	0.45	–	1.25	1.25	–	0.83	1.5	1.5
6	BL	933	60	0.45	–	1.25	1.25	–	0.83	1.5	1.5
7	BL	933	–	0.45	0.05	1.25	–	1.25	0.83	1.5	1.5
8	BL	933	–	0.45	0.10	1.25	–	1.25	0.83	1.5	1.5
9	BL	1025	15	0.45	–	1.25	1.25	–	0.83	1.5	1.5
10	BL	1025	–	0.45	0.10	1.25	–	1.25	0.83	1.5	1.5
11	NC	805	15	0.45	0.05	1.25	1.25	1.25	0.83	1.5	1.5
12	NC	805	60	0.45	0.05	1.25	1.25	1.25	0.83	1.5	1.5
13	NC	805	15	0.45	0.10	1.25	1.25	1.25	0.83	1.5	1.5
14	NC	805	60	0.45	0.10	1.25	1.25	1.25	0.83	1.5	1.5
15	NC	933	15	0.45	0.05	1.25	1.25	1.25	0.83	1.5	1.5
16	NC	933	60	0.45	0.05	1.25	1.25	1.25	0.83	1.5	1.5
17	NC	933	15	0.45	0.10	1.25	1.25	1.25	0.83	1.5	1.5
18	NC	933	60	0.45	0.10	1.25	1.25	1.25	0.83	1.5	1.5
19	NC	1025	15	0.45	0.10	1.25	1.25	1.25	0.83	1.5	1.5
20	UC	805	15	0.45	0.10	1.25	1.25	1.25	0.83	1.5	1.5
21	UC	805	60	0.45	0.10	1.25	1.25	1.25	0.83	1.5	1.5
22	UC	933	60	0.45	0.10	1.25	1.25	1.25	0.83	1.5	1.5
23	UC	1025	15	0.45	0.10	1.25	1.25	1.25	0.83	1.5	1.5

addition, Kokjohn et al. [43] found that with the presence of fuel stratification produced by the direct injection, the range of ϕ is about 0.1–0.8, which corresponds to $\phi' = 0.1$ at $\phi_0 = 0.45$. However, depending on the fuel injection process such as the inject timing and the mass ratio of PFI to DI, the corresponding $T-\phi$ distribution can vary significantly. As such, for a given ϕ' of 0, 0.05, and 0.1, three different T' of 0, 15, and 60 K are adopted. Through this choice of T' and ϕ', the ignition characteristics of *n*-heptane/air mixture under HCCI conditions can be investigated in a comprehensive manner.

The initial mean temperatures are deliberately chosen such that they lie within or near the NTC regime. Therefore, the ignition characteristics of a *n*-heptane/air mixture can be investigated in three different regimes of the low-, intermediate-, and high-temperature chemistry. In the same way, ϕ_0 and ϕ' are carefully selected to maintain local ϕ below unity as in experiments [4], which is supposed to prevent excessive NO*x* generation in real engines. The initial conditions are representative of the TDC under high-load conditions in highly air-diluted HCCI combustion [44,45]. The 0-D homogeneous ignition delay is evaluated from the 0-D simulation of a homogeneous *n*-heptane/air mixture of ϕ_0 at initial T_0 and p_0. Henceforth, τ_{ig} denotes the time at which the maximum mean HRR occurs for all 0-D and 2-D simulations. The superscript 0 represents the 0-D homogenous ignition.

An isotropic kinetic energy spectrum function by Passot and Pouquet [46] is adopted to prescribe the initial turbulent flow field as in [6–13,47–49]. The initial turbulence decays over time since the combustion occurs in a constant volume without any mean shear layer. In general, large turbulence intensity is not favored for the SCCI combustion because it can significantly homogenize mixture inhomogeneities [4,12]. Therefore, intermediate turbulence intensity, u', of 0.83 m/s and most energetic length scale, l_e, of 1.25 mm are specified to match the corresponding turbulence timescale, τ_t, of 1.5 ms, with τ_{ig}^0 and that in real HCCI engines ($\sim O(1)$ ms).

It is of interest to note that the temporal evolution of 3-D turbulence is qualitatively different from that of 2-D turbulence due to the 3-D vortex-stretching effect. However, it is still valuable to investigate HCCI combustion with 2-D turbulence because the effect of turbulent mixing on HCCI combustion is less important than that of mixture stratifications [6–11,30,36,50]. As such, it is reasonable to expect that the overall HCCI combustion characteristics of 2-D DNSs may not be very different from those of 3-D DNSs as discussed in [19,36,50]. Moreover, for many parametric DNS studies, it is more feasible to perform 2-D DNSs than extremely-expensive 3-D DNSs.

Temperature and concentration fields are also generated from the same energy spectrum as turbulence with different random number. The most energetic length scales of temperature and composition fluctuations, l_{Te} and $l_{\phi e}$, are 1.25 mm for all cases. The identical characteristic length and time scales for turbulence and scalar fields are specified and hence, most effective turbulent mixing of initial mixtures can be elucidated in the present study [10].

At the TDC prior to the main auto-ignition event, different $T-\phi$ correlations may exist due to such factors as fuel delivery strategy, injection timing, amount of EGR, intake charge heating, and wall heat loss. In the present study, two most-probable scenarios are examined as another parameter for DNSs: (1) uncorrelated (UC) $T-\phi$ fields resulting from the early direct injection in the one-stage injection in combination with EGR and turbulent mixing, and (2) negatively-correlated (NC) $T-\phi$ fields caused by the evaporative cooling of the second late-direct injection in the two-stage injection together with short mixing time [30,51]. Although the uncorrelated $T-\phi$ fields cannot be achieved without expensive intake charge heating, the UC cases are considered here to compare the effect of UC fields with that of NC fields. In addition to two $T-\phi$ correlations, cases with T' or ϕ' only are simulated to isolate their effects on the ignition although cases with ϕ' only are unrealistic. Figures 1 and 2 show several initial $T-\phi$ relations together with a representative isocontour of the initial equivalence ratio field for Case 14.

A square box of 3.2×3.2 mm^2 discretized with 1280 grid points in each direction was used for all 2-D DNSs. The fine grid resolution of 2.5 μm is required to resolve thin flame fronts generated by locally-high temperature and/or equivalence ratio and as such, the thinnest reaction layers in 2-D DNSs are resolved with at least 11–15 grid points. The 2-D DNSs were performed on the IBM Blue Gene/P of the Supercomputing Laboratory at King Abdullah University of Science and Technology (KAUST). Each of the DNSs required approximately 0.8 million CPU-hours.

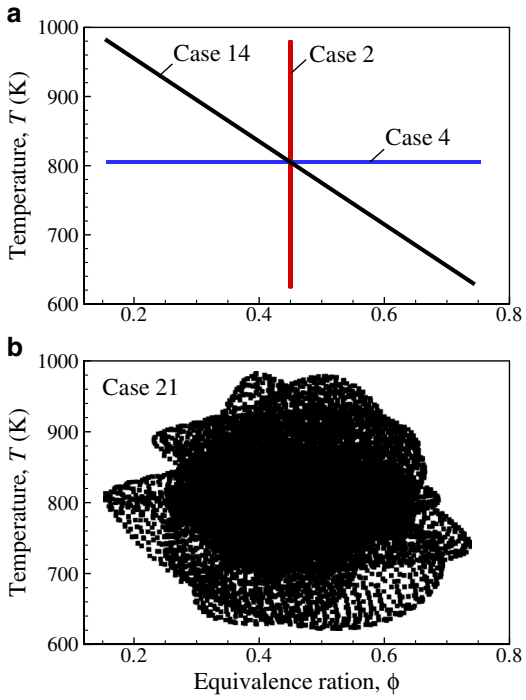

Fig. 1. Initial $T-\phi$ distribution for (a) Cases 2, 7, 14 and (b) Case 21.

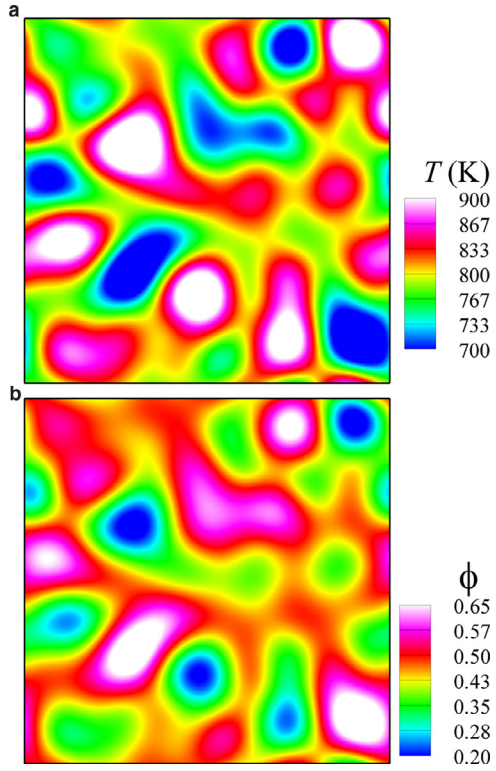

Fig. 2. Initial field of (a) temperature and (b) equivalence ratio for Case 14.

3. Effects of T' and ϕ' at different T_0

3.1. 0-D ignition characteristics

In general, HCCI combustion is believed to occur through volumetric auto-ignition and as such, the characteristics of the 0-D ignition delay, τ_{ig}^0, of lean *n*-heptane/air mixtures is first examined here

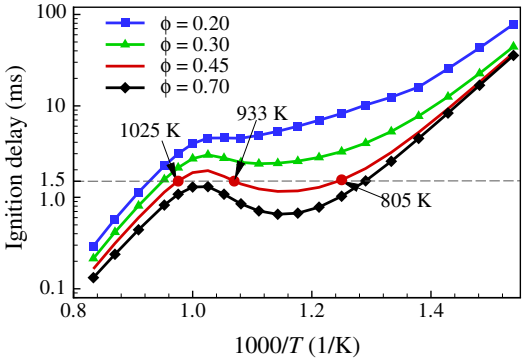

Fig. 3. 0-D ignition delay of *n*-heptane/air mixtures as a function of initial temperature for different ϕ_0 at $p_0 = 40$ atm.

to gain an insight into the effects of T' and ϕ' on *n*-heptane HCCI combustion. Figure 3 shows the 0-D ignition delay of lean *n*-heptane/air mixtures with different ϕ_0 as a function of T_0 at $p_0 = 40$ atm. It is readily observed from Fig. 3 that for the low and high temperature regimes outside the NTC regime ($T_0 < 800$ K or $T_0 > 1000$ K), τ_{ig}^0 is more sensitive to T_0 than ϕ_0. However, for T_0 within/near the NTC regime (800 K $< T_0 <$ 1000 K), τ_{ig}^0 is more sensitive to ϕ_0 than T_0 compared to the low and high temperature regimes. This is primarily because the NTC regime occurs within the intermediate-temperature range (e.g., 875 K $< T_0 <$ 975 K for $\phi_0 = 0.45$), where the low/intermediate temperature heat release advances the second-stage ignition more in time with decreasing T_0 such that τ_{ig}^0 is relatively constant. Moreover, it is further attributed to the strong NTC behavior at relatively-large ϕ_0. This strong NTC behavior occurs because the temperature increase induced by the first-stage ignition becomes significant at relatively-large ϕ_0, resulting in the advancement of the second-stage ignition.

The sensitivity of the ignition of hydrocarbon/air mixtures to temperature and composition variations under HCCI conditions has been reported in many previous numerical and experimental studies [9,12,14,15,17,23,52]. For example, in 2-D DNSs of the ignition of *n*-heptane/air mixture [9], it was found that the overall combustion proceeds in different ways depending on the relative location of T_0 to the NTC regime and the degree of T'. It was also reported from [12,14,15] that the HCCI combustion of high-reactivity fuel/air mixture exhibiting two-stage ignition (e.g., diesel, PRF73, and *n*-heptane) is highly sensitive to mixture stratification. For low-reactivity fuel/air mixture with only one-stage ignition (e.g., gasoline, *iso*-octane, and ethanol), the overall combustion is less sensitive to fuel stratification under naturally aspirated HCCI conditions [14,15,17,23,52]. However, it was found that under boosted intake pressure, the HCCI combustion of gasoline/air mixture becomes highly sensitive to fuel stratification [22,53,54].

All of these different ignition characteristics under HCCI conditions are primarily attributed to initial mixture conditions such as mean temperature and equivalence ratio from which the overall combustion can go through different reaction pathways: low-, intermediate-, and high-temperature chemistry. In the following sections, therefore, the overall ignition characteristics of thermally and/or compositionally stratified *n*-heptane/air mixture with different $T-\phi$ correlations are elucidated at three different T_0, which may involve different reaction pathways.

3.2. Effects of T' or ϕ' at different T_0: BL cases

To elucidate the effect of temperature or composition fluctuation only on the overall ignition characteristics of *n*-heptane/air mixture under HCCI conditions, 10 baseline (BL) cases with either T' only or

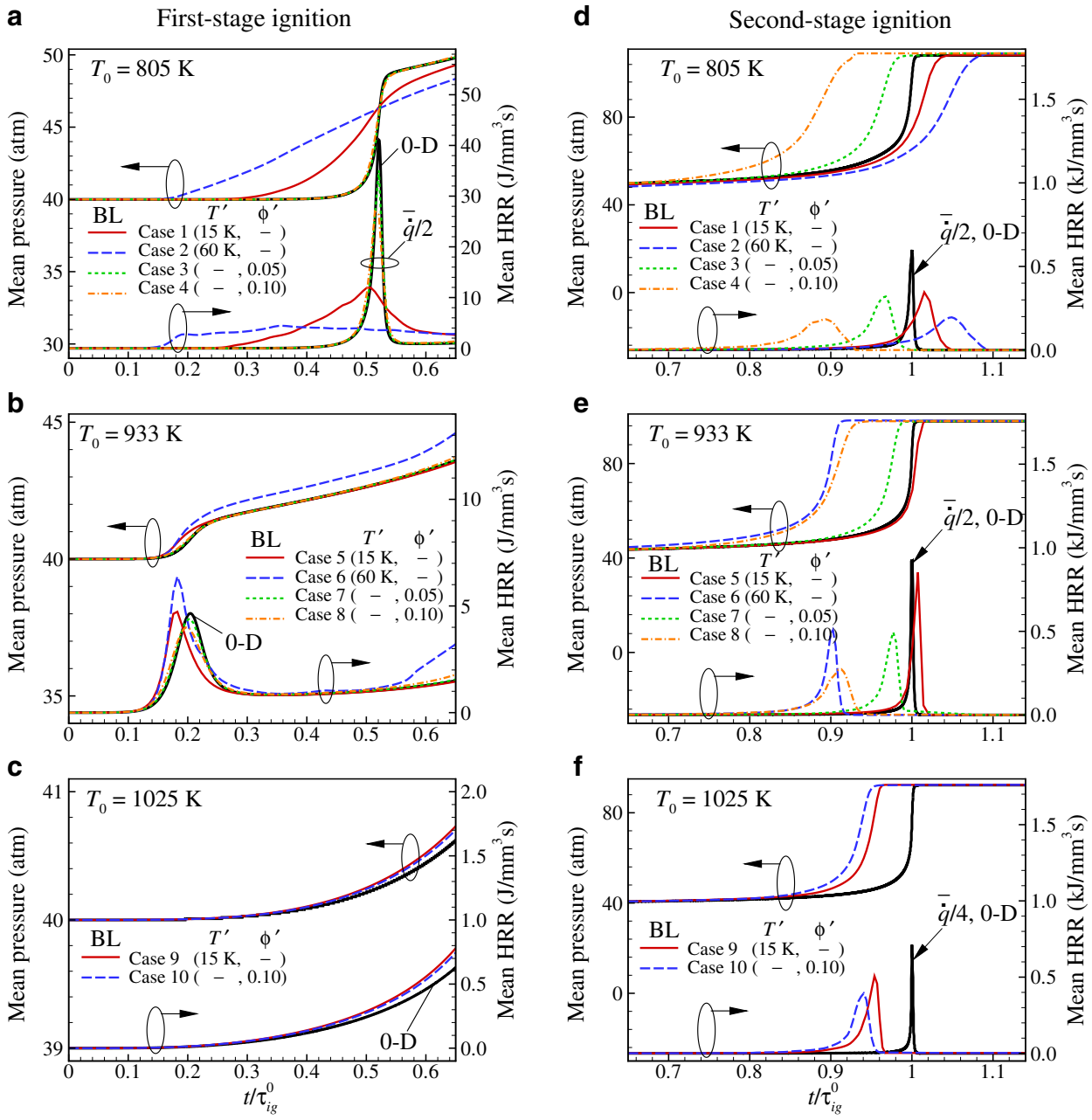

Fig. 4. Temporal evolutions of the mean pressure and mean HRR for the BL cases with $T_0 = 805$ K (a and d), $T_0 = 933$ K (b and e), and $T_0 = 1025$ K (c and f) during the first-stage (left) and second-stage (right) ignition.

ϕ' only are examined. Figure 4 shows the temporal evolution of mean pressure, $\bar{p}$, and mean HRR, $\bar{\dot{q}}$, for the BL cases (Cases 1–10) together with the corresponding 0-D homogeneous ignitions during the first- and second-stage ignition. Note that unlike cases with $T_0 = 805$ and 933 K, cases with $T_0 = 1025$ K have no first-stage ignition due to their relatively-high T_0 as shown in Fig. 4c; their ignition process is thus solely determined by the transition from the intermediate-temperature to high-temperature chemistry.

3.2.1. First-stage ignition: BL cases

For the BL cases with $T_0 = 805$ K (Cases 1–4), it is readily observed from Fig. 4a that $\bar{\dot{q}}$ is more spread out over time and its peak is significantly reduced with increasing T' but they do not change much with increasing ϕ' compared to their corresponding values of 0-D ignition. This is primarily because the first-stage ignition is governed by the low-temperature chemistry which is more sensitive to T than ϕ as mentioned above. Moreover, under the present initial conditions, the first-stage ignition delay, $\tau^0_{ig,1}$, is much shorter than the turbulence timescale, τ_t ($= \tau^0_{ig}$), and as such, the effect of turbulent mixing on the first-stage ignition is negligible. This implies that the first-stage ignitions of local mixtures with different T (Cases 1 and 2) occur spontaneously with wide time difference, resulting in the temporal spread of $\bar{\dot{q}}$. On the contrary, local mixtures with different ϕ (Cases 3 and 4) ignite simultaneously at the same time and as such, the overall first-stage ignition proceeds similarly to the 0-D ignition.

For $T_0 = 933$ K (Cases 5–8) in Fig. 4b, however, the overall first-stage ignitions are quite similar to the 0-D ignition regardless of T' and ϕ'. From many 0-D ignition simulations, it is found that unlike cases at $T_0 = 805$ K, $\tau^0_{ig,1}$ remains nearly the same for different T_0 around 933 K. This is because the strength of the first-stage ignition manifested in the maximum HRR is significantly reduced with increasing T_0 and as such, the effect of T_0 on the first-stage ignition

becomes significantly limited. Moreover, the first-stage ignition does not change much with ϕ as discussed above and as such, the overall first-stage ignition for cases with T' only or ϕ' only proceeds similarly to the corresponding 0-D ignition. In summary, the first-stage ignitions of local mixtures occur spontaneously with only time difference due to $\tau^0_{ig,1} < \tau_t$ and T' has a first-order effect on the first-stage ignition at low T_0 in which strong first-stage ignition occurs.

3.2.2. Second-stage ignition: BL cases

For the characteristics of the second-stage ignition of the BL cases, several observations are made from Fig. 4d–f. First, $\bar{\dot{q}}$ is more spread out over time and its peak is more decreased with increasing T' or ϕ' for all cases regardless of T_0. These results are attributed to the general effects of temperature and composition stratifications found in many previous DNS studies [6,8–13,35]; as the degree of T' or ϕ' is increased, the deflagration mode of combustion rather than the spontaneous ignition mode prevails during the main combustion event, resulting in the reduction of the peak $\bar{\dot{q}}$.

Second, the ignition delay, τ_{ig}, behaves non-monotonically with T' (Cases 1, 2, 5, 6, and 9) at different T_0 but it is always decreased with increasing ϕ' regardless of T_0 (Cases 3, 4, 7, 8, and 10). More specifically, as T' is increased, τ_{ig} is increased for low T_0 of 805 K; whereas, it is decreased for high T_0 of 1025 K. For intermediate T_0 of 933 K, however, τ_{ig} is slightly increased with small T', while being decreased with large T', exhibiting the combined effects of both low and high T_0 near the NTC regime as found in [9].

These ignition characteristics can simply be understood by examining the distribution of τ^0_{ig} of initial fields as demonstrated in [9,12,13]. Figure 5 shows the 95% range of τ^0_{ig} for the initial mixture fields for the BL cases. The 95% range of τ^0_{ig} represents the span of τ^0_{ig} in the initial mixture, wherein T and ϕ lie within 95% of the range of each parameter centered at T_0 and ϕ_0. Note that local mixture with the shortest τ^0_{ig} is more likely to auto-ignite first and as such, it may determine the start of the main combustion, while the span of τ^0_{ig} may decide the duration of the main combustion. Nascent ignition kernels from mixtures with the shortest τ^0_{ig} develop into wave-like fronts and propagate to consume adjacent unburnt fuel/air mixtures. Meanwhile, new ignition kernels also develop due to increased temperature and pressure, which leads to a sequential ignition process by the combustion mode of deflagration and/or the mode of spontaneous ignition.

As shown in Fig. 5, the shortest τ^0_{ig} and its 95% range become smaller and larger, respectively with increasing T' or ϕ'. As such, the start of the main combustion can be advanced in time and its duration can be prolonged, consequently spreading out the mean HRR over time. However, the overall combustion for Case 4 is finished much later than that for Case 2 and even that for the 0-D ignition. This is because most of local mixtures in Case 4 have much longer ignition delay than τ^0_{ig} and hence, they are mainly consumed by the deflagration mode of combustion, which leads to the significant retardation of the overall combustion compared to 0-D ignition. Moreover, since the turbulent timescale is nearly identical to the fastest τ^0_{ig} of the mixtures, significant turbulent mixing can also delay the overall combustion by dissipating heat and radicals in nascent ignition kernels. However, the range of τ^0_{ig} for Case 5 in Fig. 5b is narrow and their values are nearly comparable to the 0-D ignition delay. As such, their overall combustion becomes more like 0-D ignition as shown in Fig. 4b.

It is also readily observed from Fig. 4 that unlike the cases with T' only, the overall combustion of the BL cases with ϕ' only (Cases 3, 4, 7, 8, and 10) is advanced in time and the duration of the main combustion is prolonged with increasing ϕ' regardless of T_0. The BL cases with ϕ' only involve relatively-wide range of τ^0_{ig} and mixtures with shorter ignition delays compared to the corresponding 0-D ignition as shown in Fig. 5. Therefore, deflagrations rather than spontaneous ignition evolve earlier than τ^0_{ig} and propagate into adjacent unburnt mixtures, resulting in the advancement of the overall combustion and distribution of the mean HRR. It is also of interest to note that when T_0 lies within the high temperature regime (Case 10 with $T_0 = 1025$ K), wherein the overall combustion is primarily governed by the high-temperature chemistry, fuel stratification becomes less effective in reducing the peak $\bar{\dot{q}}$ and advancing τ_{ig}. Moreover, in this high temperature regime, small T' induces quite similar result to that by large ϕ' in terms of the advancement of the overall combustion [9,12].

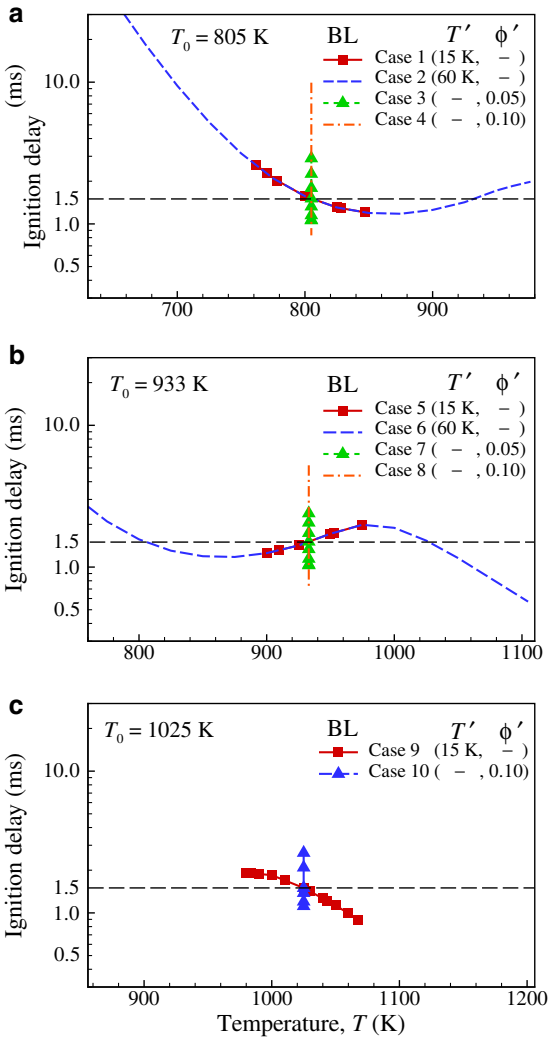

Fig. 5. The 95% range of τ^0_{ig} for the BL cases with (a) $T_0 = 805$ K, (b) $T_0 = 933$ K, and (c) $T_0 = 1025$ K.

3.3. Effects of negatively-correlated $T - \phi$ fields: NC cases

To understand the effect of two different $T - \phi$ correlations on the ignition of n-heptane/air mixture, the temporal evolution of the mean HRR for the negatively-correlated (NC) and uncorrelated (UC) cases at three different T_0 is shown in Fig. 6 together with the BL cases. During the first-stage ignition, the overall combustion for all NC and UC cases proceeds quite similarly to that of the BL cases with the same T' regardless of ϕ'. As discussed above, this is because the first-stage ignition is mainly determined by the low-temperature chemistry sensitive to temperature variation, and is not affected by turbulence mixing of which timescale, τ_t, is much longer than $\tau^0_{ig,1}$.

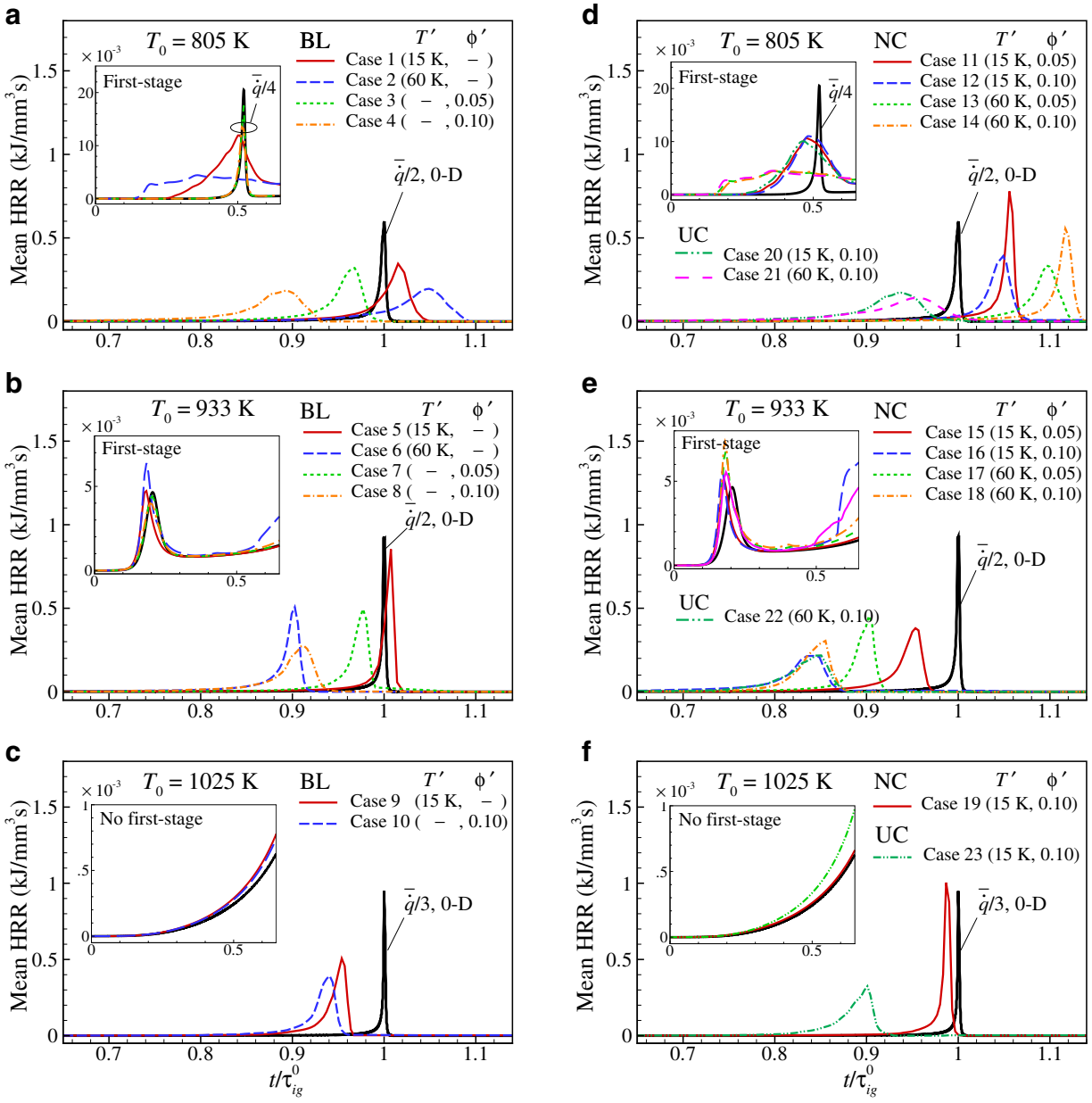

Fig. 6. Temporal evolutions of the mean HRR for the BL (left column) and NC and UC (right column) cases with $T_0 = 805$ K (a and d), $T_0 = 933$ K (b and e), and $T_0 = 1025$ K (c and f) during the second-stage ignition. The first-stage ignitions are shown in the small boxes.

For the second-stage ignition of the NC cases, several points are to be noted from Fig. 6d–f. First, for cases with $T_0 = 805$ K and 1025 K, the negative $T - \phi$ correlation has an adverse effect on the overall combustion in terms of HRR distribution; the peak $\bar{q}$ is significantly increased and the duration of the main combustion is reduced compared to those of the BL cases. In addition, the overall combustion is finished much later than that of the corresponding BL case.

These results are primarily attributed to the characteristics of the 0-D ignition delays of initial mixtures and the turbulence timescale relative to τ^0_{ig}. As shown in Fig. 7a and c, the 0-D ignition delays for Cases 11 and 19 spans relatively-narrow range close to 1.5 ms such that the overall combustion may occur by the spontaneous ignition even though it is slightly delayed for Case 11 and advanced for Case 19. Moreover, the turbulent timescale is similar to the 0-D ignition delays for the cases and hence, turbulence can effectively homogenize the initial mixture, resulting in the retardation of the overall combustion. For Cases 12–14, the 0-D ignition delays of most mixtures are much greater than 1.5 ms and as such, turbulence with τ_t of 1.5 ms can dissipate effectively heat and radicals from nascent ignition kernels and homogenize mixtures. As a result, the overall combustion is retarded. These results verify that the positive effects of temperature inhomogeneities in the initial mixture on the HCCI combustion can be diminished by fuel stratification if it is introduced into the engine cylinder opposite to thermal stratification, leading to rapid volumetric ignition [12,28–30].

Second, for cases with intermediate T_0 of 933 K (see Fig. 6e), the negative correlation of $T - \phi$ fields has a positive effect on the overall combustion by spreading out $\bar{q}$ over time and reducing the peak $\bar{q}$. These results can also be understood by examining 0-D ignition delays of initial mixtures. As shown in Fig. 7b, the negatively-correlated $T - \phi$ fields for Cases 15–18 induce much shorter 0-D ignition delays of the initial fields than τ^0_{ig} of 1.5 ms. Therefore, it can be expected that nascent ignition kernels can successfully develop into deflagrations, which consequently advance the overall combustion and distribute

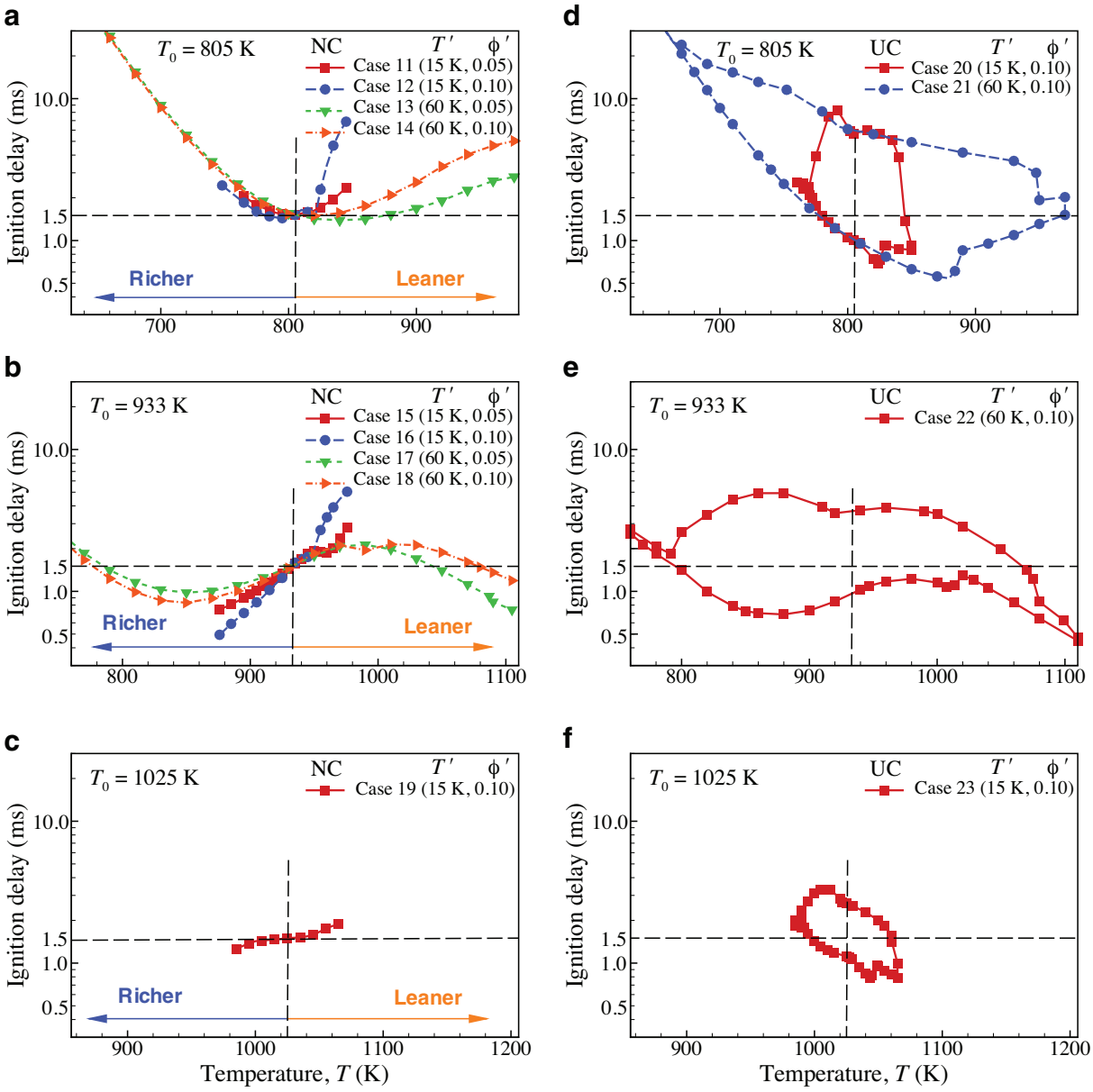

Fig. 7. The 95% range of τ_{ig}^0 for the NC (left) and UC (right) cases with $T_0 = 805$ K (a and d), $T_0 = 933$ K (b and e), and $T_0 = 1025$ K (c and f).

the mean HRR over time. Moreover, for cases with the same T', the shortest 0-D ignition delay for $\phi' = 0.10$ is much smaller than that for small ϕ' of 0.05 and as such, the overall combustion is more advanced with large ϕ' for cases with same T'.

It is of interest to note from Fig. 7b that for cases with $\phi' = 0.10$, the shortest 0-D ignition delay for Case 16 is much smaller than that for Case 18 and as such, it may be expected that the overall combustion for Case 16 is finished much earlier than that for Case 18. In reality, however, the overall combustion of the two cases proceeds quite similarly to each other. The characteristics of overall combustion may be determined not only by the shortest 0-D ignition delay but also by the number of ignition kernels which can successfully develop into deflagrations.

To further elucidate the ignition characteristics of the NC cases at $T_0 = 933$ K, the instantaneous isocontours of HRR field at the times of 5%, 50%, and 95% cumulative $\bar{q}$, and the maximum $\bar{q}$ are shown in Fig. 8. The local HRR, $\dot{q}$, is normalized by the maximum HRR of the corresponding 0-D ignition, $\dot{q}_m^0 = 1857$ J/mm^3 s. For Case 16, deflagration waves emanate from nascent ignition kernels much earlier than those for the other cases because the shortest 0-D ignition delays in Case 16 is smaller than those in other cases. For Cases 16 and 18, however, the temporal evolution of $\bar{q}$ are not quite different. At time of 5% cumulative $\bar{q}$, more corrugated deflagration waves are observed for Case 18 than for Case 16, implying that Case 18 has more nascent ignition kernels which ultimately develop into deflagrations than Case 16.

This qualitative observation can be verified by examining the probability density function (PDF) of τ_{ig}^0 and its spatial gradient, $|\nabla\tau_{ig}^0|$, of initial mixtures as shown in Fig. 9. It is readily observed that only the PDF of τ_{ig}^0 of Case 16 exhibits non-zero values near $\tau_{ig}^0 = 0.5$ ms and the PDF of τ_{ig}^0 of Case 18 has a peak at $\tau_{ig}^0 = 0.95$ ms, which is greater than those of other cases. These results imply that even though the ignition kernels start to develop earlier in Case 16 than in Case 18, more deflagrations in Case 18 consume unburnt mixtures faster than in Case 16. Therefore, the overall combustion of the two cases proceeds similarly to each other. It is also observed from the figure that the PDF of $|\nabla\tau_{ig}^0|$ of Case 18 is slightly more distributed up to very large $|\nabla\tau_{ig}^0|$ than that of Case 16, which implies that once

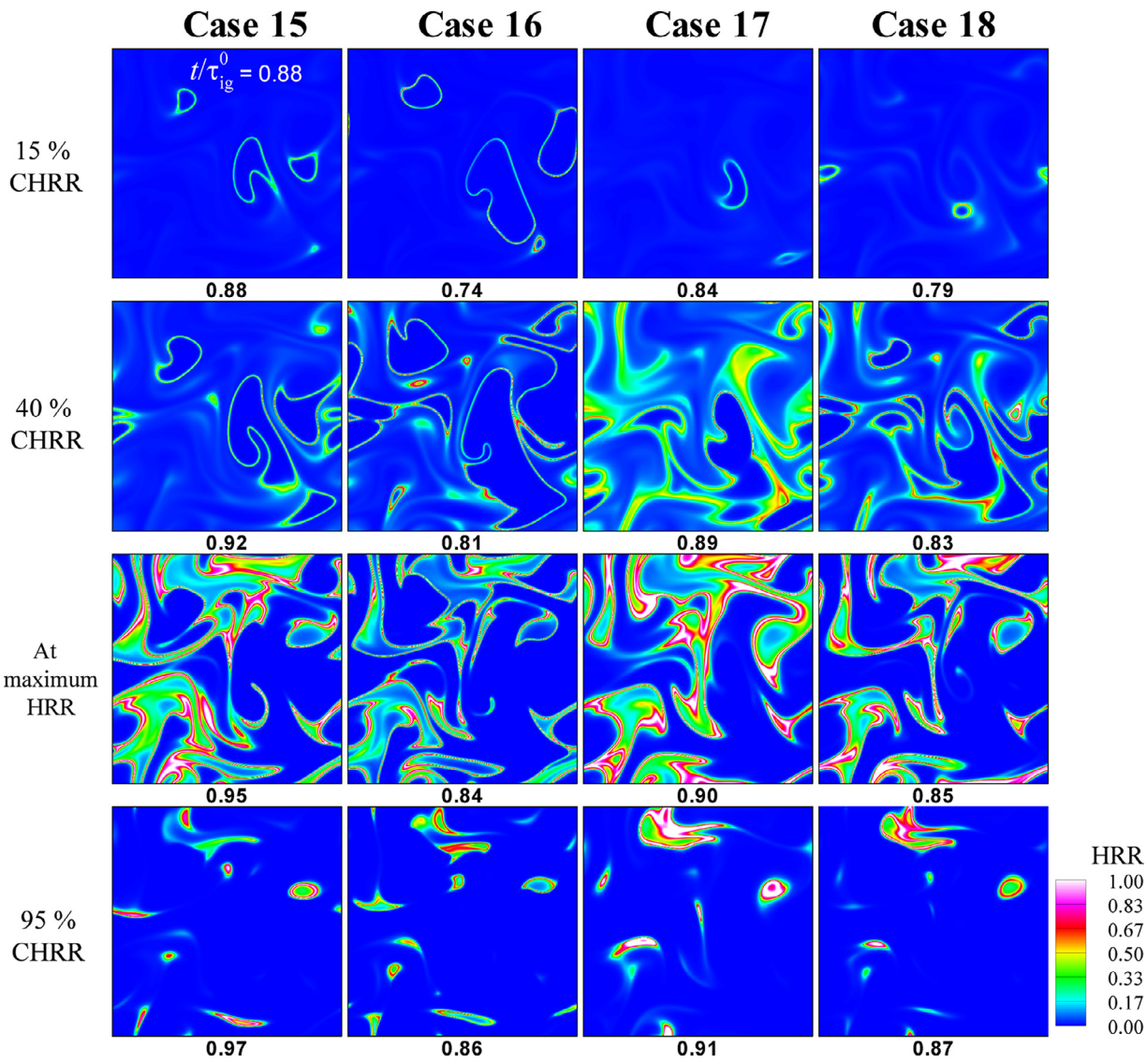

Fig. 8. Isocontours of normalized HRR for Cases 15–18 (from left to right) at times of 15% (first row), 40% (second row), and 95% (last row) cumulative mean HRR and at the maximum HRR (third row).

deflagration waves are developed, the deflagration mode can prevail more in Case 18. The characteristics of deflagration mode of combustion are further discussed in the next section.

For the cases with small ϕ' of 0.05 (Cases 15 and 17), however, large T' tends to advance the overall HCCI combustion and increase the peak $\bar{q}$ sightly. In addition, for cases with the same ϕ', τ_{ig} for the negatively-correlated cases are shorter than those of the corresponding BL cases with ϕ' only (Cases 8 and 9); for example, τ_{ig} for the BL case (Case 9) and negatively-correlated cases (Cases 16 and 18) are approximately 0.91 and 0.85, respectively. Furthermore, as shown in Fig. 9, the PDFs of τ_{ig}^0 and $|\nabla\tau_{ig}^0|$ of Case 17 are more distributed than those of Case 15 and as such, the deflagration mode is expected to prevail more in Case 17 than Case 15. All of these results imply that negatively-correlated $T-\phi$ fields at intermediate T_0 within the NTC regime have a synergistic effect of advancing the overall combustion and smoothing out the PRR and HRR under high-load HCCI combustion.

3.4. Effects of uncorrelated $T-\phi$ fields: UC cases

As mentioned above, the uncorrelated $T-\phi$ distribution prior to the main combustion event is another scenario which may occur in HCCI combustion [12,30]. For completeness, four cases with uncorrelated $T-\phi$ distribution (Cases 20–23) are examined to understand the combined effects of temperature and composition inhomogeneities in/near the NTC regime on the overall HCCI combustion.

Several observations can be made for the UC cases from Fig. 6d–f. Unlike the NC cases, the overall combustion of all UC cases is more advanced in time and the duration of the main combustion is further increased regardless of T_0 compared to their corresponding 0-D ignition. The 95% range of 0-D ignition delay for the UC cases (see Fig. 7d–f) can further identify the ignition characteristics of the UC cases; the overall HCCI combustion occurs rapidly because the fastest ignition delay is much shorter than $\tau_{ig}^0 = 1.5$ ms and the mean HRR is more distributed over time due to the wide spread of ignition delay.

Even though the overall combustion characteristics for all UC cases seem to be analogous in many ways, different behaviors of the overall combustion for different T_0 can be observed. For cases with $T_0 = 805$ K (Cases 20 and 21), the temporal distribution of the mean HRR by uncorrelated $T-\phi$ field becomes more significant than the corresponding BL cases with ϕ' only (Cases 3 and 4), which is primarily attributed to the wider range of ignition delay of the UC cases. In the same context, uncorrelated large T' and ϕ' in Case 21 tend to retard the overall combustion compared to Case 4 with ϕ' only. The

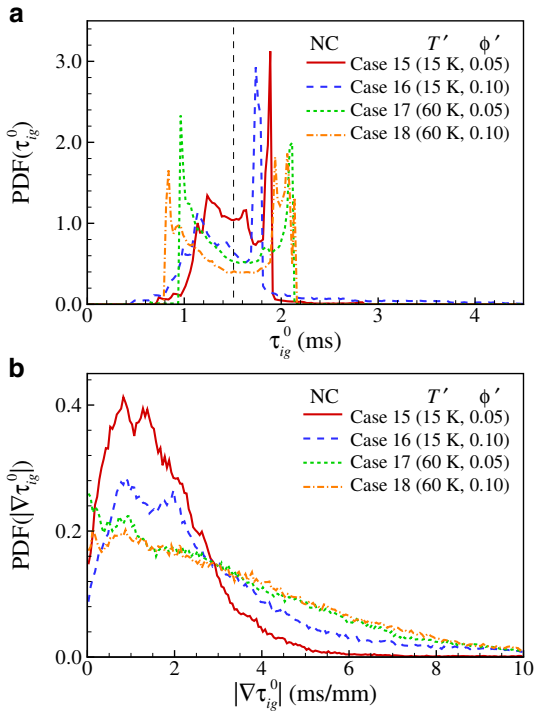

Fig. 9. The probability density function of (a) 0-D ignition delay and (b) its spatial gradient of initial mixtures for Cases 15–18.

occurrence of ignition kernels and their development into deflagrations happens at the same time due to their similar fastest ignition delay. However, it takes more time to consume the whole fuel/air mixture of Case 21 with wide range of ignition delay than does Case 4 with relatively narrow range of ignition delay.

However, for cases with $T_0 = 933$ K (Case 22) and 1025 K (Case 23), the uncorrelated $T-\phi$ fields advance the overall combustion and spread out the mean HRR compared to the BL cases with T' only or ϕ' only, which is also attributed to the shorter fastest ignition delays and wide range of ignition delay in the initial fuel/air mixture. For Case 22, moreover, the effect of uncorrelated $T-\phi$ field becomes comparable to that of negatively-correlated $T-\phi$ field because in the NTC regime, the 95% range of ignition delay for the UC cases becomes comparable to that for the NC cases and as such, the overall HCCI combustion of the UC case proceeds similarly to that of the NC cases. In summary, the uncorrelated $T-\phi$ distribution has a synergetic effect in preventing excessive PRR by temporally distributing $\bar{q}$ compared to the BL cases with T' only or ϕ' only.

3.5. Combustion mode

In the previous sections, the spontaneous ignition and deflagration modes of combustion are discussed without any quantitative analysis. As such, in this section, the occurrence of deflagration mode during combustion is quantitatively measured by adopting the Damköhler number, *Da*, defined as [9–12,55,56]:

$$Da = \frac{\dot{\omega}_k}{|-\nabla\cdot(\rho Y_k \mathbf{V}_k)|}, \tag{1}$$

where Y_k, $\mathbf{V}_k$, and $\dot{\omega}_k$ denote the mass fraction, diffusion velocity, and net production rate of species k, respectively. $Y_c \equiv Y_{CO_2} + Y_{CO}$ is used for the Damköhler number analysis.

To delineate between the deflagration and spontaneous ignition modes, *Da* in the diffusive limit is identified from a series of 1-D laminar simulations at various ϕ_0. Note that the diffusive limit represents a condition in which deflagration wave propagates without auto-ignition or diffusion balances reaction [7–12]. From the simulations, it is found that *Da* in the diffusive limit is approximately 2.0. Note that in the diffusive limit under the present specific conditions, *Da* becomes larger than unity because the mixture upstream of the deflagration wave is highly reactive, and as such, the reaction term of *Da* becomes larger than the diffusion term [9–12]. In the present study, combustion is determined to occur by the deflagration mode when the corresponding *Da* is less than 2.0.

Figure 10 shows the temporal evolution of the fraction of HRR from the deflagration mode for all DNS cases. It is readily observed that prior to the main ignition, most of heat release occurs in the deflagration mode except for Cases 1, 5, 11, and 19 in which T' and/or ϕ' are relatively small. It is also found that in most cases, the fraction of HRR from the deflagration mode is rapidly reduced near the occurrence of the peak $\bar{q}$. These results verify that for large T' and/or ϕ' cases, combustion occurs primarily by the deflagration mode during the early stage of ignition; however, the mixed mode of deflagration and spontaneous ignition takes it over during the main combustion process. Note that at the final stage of ignition, the fraction of HRR from the deflagration mode increases up to unity because $\dot{\omega}_c$ in Eq. (1) vanishes, consequently leading to $Da = 0$.

To further identify the effect of deflagration mode on the characteristics of HCCI/SCCI combustion, the maximum HRR, burning duration, and total HRR fraction from the deflagration mode for all DNS cases are listed in Table 2. In general, the total HRR fraction from the deflagration mode is increased with increasing T' and/or ϕ', resulting in the reduction of the maximum HRR and the increase of the burning duration. For the NC cases (Cases 12 vs. 14, 15 vs. 17, and 16 vs. 18), however, the total fraction of HRR is reduced when T' is increased from 15 K to 60 K. As T' is increased, more mixtures outside the NTC regime are included in the initial field and as such, the canceling effect of negatively-correlated $T-\phi$ fields outside the NTC regime is enhanced and the first order effect of ϕ' on the HCCI combustion is slightly reduced.

In summary, deflagration waves can successfully develop at the early stage of combustion only if the shortest τ^0_{ig} of initial mixture induced by large T' and/or ϕ' is small enough. This early development of deflagrations can render relatively-large portion of combustion to occur by the deflagration mode, which significantly contributes to the temporal spreading of the mean HRR, and the reduction of the peak $\bar{q}$ and τ_{ig} as shown in Table 2.

4. Chemical aspects of the ignition

In this section, the effects of the initial mean temperatures and temperature/composition stratifications on the overall HCCI combustion are further elucidated by examining the temporal evolution of important species together with the overall reaction pathways of *n*-heptane oxidation. Moreover, the spatial characteristics of the ignition are also identified by chemical explosive mode analysis (CEMA).

4.1. Characteristics of temporal species evolution

Prior to analyzing the characteristics of important species, the overall reaction pathways of *n*-heptane oxidation relevant to HCCI combustion are first discussed to obtain the insight of the chemical aspects of HCCI combustion. Readers are referred to Fig. 11 for a schematic of the reaction pathways composed of three different routes: low-, intermediate-, and high-temperature chemistry [57–60].

The low-temperature chemistry of *n*-heptane oxidation is first initiated by the H-atom abstraction from a fuel molecule, RH, reacting with molecular oxygen ($RH + O_2 \rightarrow R + HO_2$). As such, HO_2 increases significantly as a result of rapid *n*-heptane decomposition during the first-stage ignition. Alkyl radical, R, then reacts with O_2 to produce

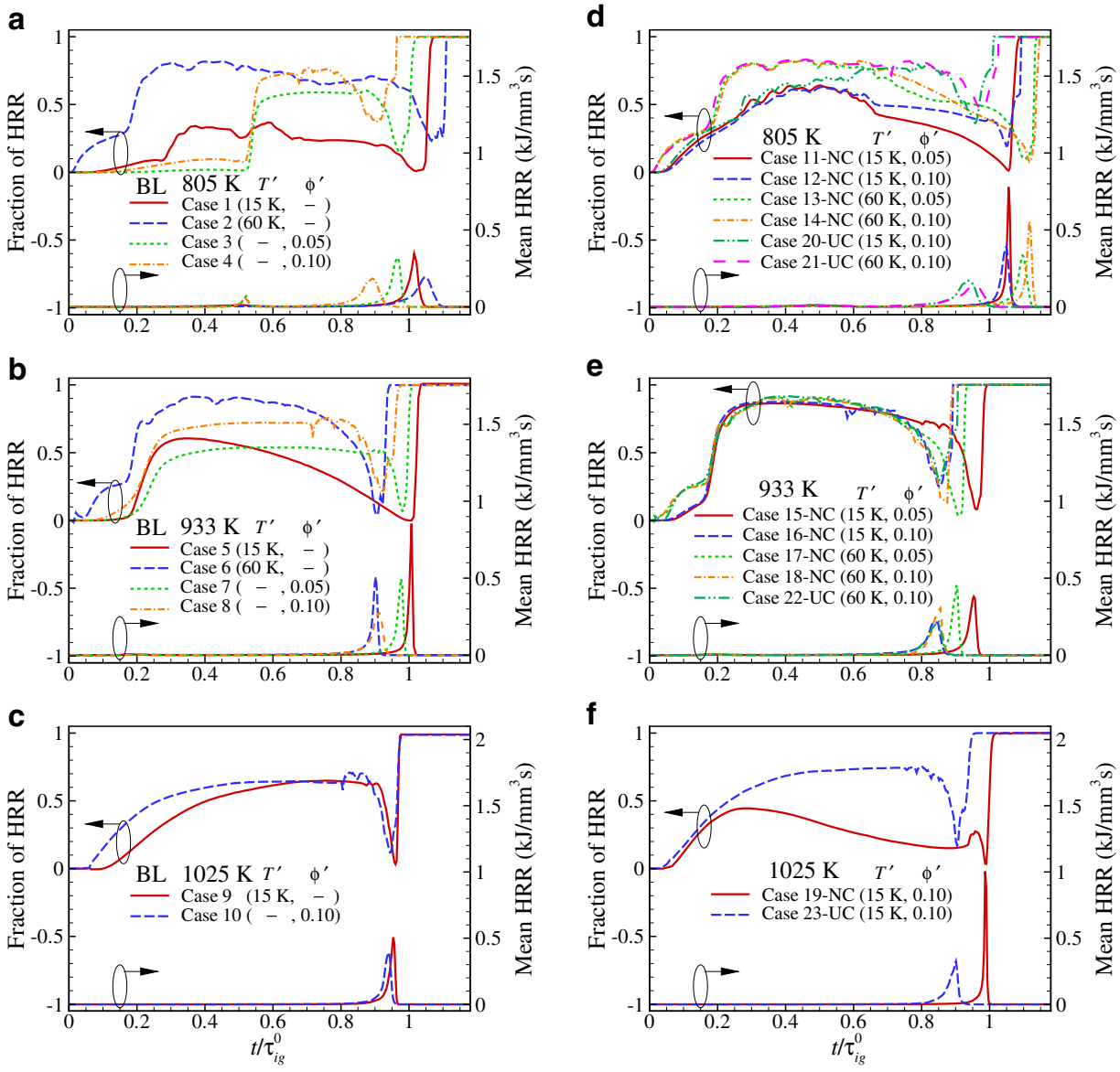

Fig. 10. Temporal evolution of the fraction of heat release rate from the deflagration mode and mean heat release rate for the BL (left) and NC/UC (right) cases.

alkylperoxy radical, RO_2, via R + O_2 + M → RO_2 + M. The rate of addition of O_2 to alkyl radical and its equilibrium depend strongly on pressure, temperature, and equivalence ratio and hence, the temperature threshold for separating the low- and high-temperature reaction path varies depending on specific conditions. Next, RO_2 radical isomerization occurs to form hydroperoxyalkyl, QOOH, (RO_2 ⇆ QOOH) followed by another O_2 addition (QOOH + O_2 → O_2QOOH). The overall rate of the low-temperature chemistry is primarily controlled by the rate of chain branching reactions through the production and decomposition of keto-hydroperoxide, KOOH; i.e., O_2QOOH → KOOH + OH and KOOH → OH + KO.

The low-temperature reaction cycle is suppressed when temperature exceeds a critical value at which the competing reaction (R + O_2 → olefin + HO_2) terminates the first-stage ignition. Between the first- and second-stage ignition, the intermediate-temperature chemistry, which is actually the combination of the low- and high-temperature chemistry, dominates the ignition of *n*-heptane/air mixture; alkyl radical and hydroperoxyalkyl species convert into the other fuel species (e.g., cyclic ether species, olefins, and ketenes) plus OH and HO_2. In this period, the rate of temperature increase is significantly reduced due to a lower reactivity of the system. Over a certain temperature threshold, the chain-branching reaction of hydrogen peroxide (H_2O_2 + M → OH + OH + M) becomes highly reactive, resulting in large enough temperature increase to initiate the chain branching reactions at high temperatures, controlled by H + O_2 → O + OH. At this point, the high-temperature chemistry becomes predominant over the low-temperature chemistry and the second-stage ignition starts to occur.

The high-temperature chemistry of *n*-heptane oxidation can be simply understood as a process of sequential decomposition of large fuel species to small fragments, down to CH_2O, HCO, H_2O_2, HO_2, CO, etc. At the final stage of the ignition, therefore, reaction pathways involve the core of H_2/CO oxidation mechanism [57,60].

Based on the above discussion of the overall reaction pathways, the temporal evolution of the mean mass fraction of important species (e.g., *n*-C_7H_{16}, HO_2, H_2O_2, OH, CO, and CO_2) and the mean HRR is shown in Figs. 12–14 for DNS cases at three different T_0 together with their corresponding 0-D ignition cases. Three distinct behaviors of the species are readily observed from the figures depending on T_0.

Table 2
Quantitative data of the DNS cases. $\bar{\dot{q}}_m$ is the maximum mean HRR; τ_{bd} is the burn duration which represents the period from 10% to 90% cumulative HRR; $\bar{\dot{q}}_{def}$ is the total fraction of HRR from the deflagration mode.

Case	Type	T_0 (K)	T' (K)	ϕ'	τ_{ig}/τ_{ig}^0	$\bar{\dot{q}}_m/\dot{q}_m^0$	τ_{bd}/τ_{ig}^0	$\bar{\dot{q}}_{def}$ (%)
1	BL	805	15	–	1.02	0.29	0.12	9.3
2	BL	805	60	–	1.05	0.16	0.15	47.2
3	BL	805	–	0.05	0.97	0.27	0.12	28.3
4	BL	805	–	0.10	0.89	0.15	0.15	46.0
5	BL	933	15	–	1.01	0.46	0.07	4.8
6	BL	933	60	–	0.90	0.27	0.09	28.2
7	BL	933	–	0.05	0.98	0.27	0.09	23.2
8	BL	933	–	0.10	0.91	0.15	0.10	40.6
9	BL	1025	15	–	0.95	0.18	0.05	27.1
10	BL	1025	–	0.10	0.94	0.14	0.07	31.4
11	NC	805	15	0.05	1.06	0.65	0.10	14.9
12	NC	805	15	0.10	1.05	0.33	0.12	33.1
13	NC	805	60	0.05	1.10	0.28	0.14	29.0
14	NC	805	60	0.10	1.12	0.46	0.11	25.6
15	NC	933	15	0.05	0.95	0.20	0.08	32.5
16	NC	933	15	0.10	0.84	0.12	0.13	48.1
17	NC	933	60	0.05	0.90	0.24	0.07	24.6
18	NC	933	60	0.10	0.86	0.16	0.11	38.7
19	NC	1025	15	0.10	0.99	0.35	0.04	11.9
20	UC	805	15	0.10	0.94	0.14	0.15	56.8
21	UC	805	60	0.10	0.95	0.12	0.17	64.3
22	UC	933	60	0.10	0.85	0.12	0.13	49.9
23	UC	1025	15	0.10	0.90	0.11	0.13	44.9

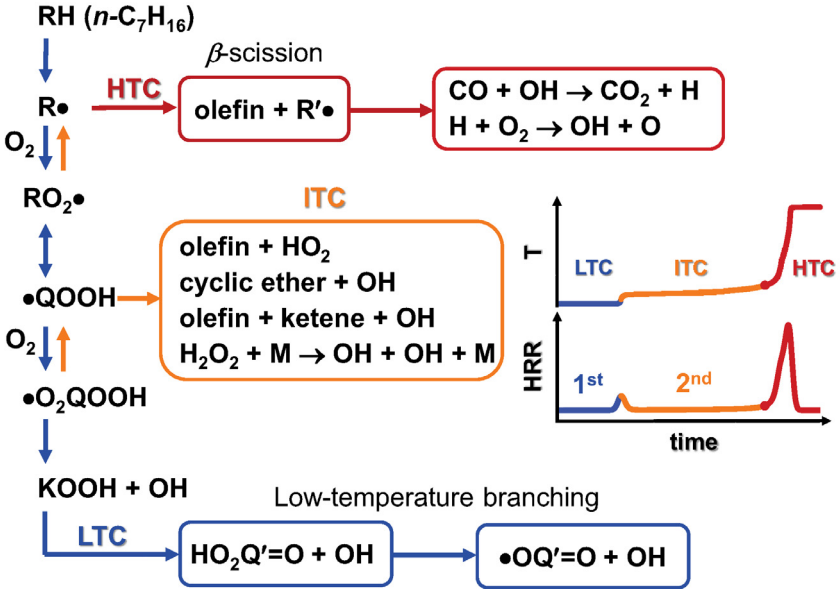

Fig. 11. Schematic of reaction pathways of *n*-heptane oxidation at different temperatures [57].

First, for Cases 4 and 11 (see Fig. 12c and d), almost all *n*-heptane is rapidly consumed by the low-temperature chemistry (RH + O_2 → R + HO_2) and as such, HO_2 mass fraction increases significantly and has its first peak during the first-stage ignition, which is similar to their corresponding 0-D case with T_0 = 805 K. Since T' for Cases 4 and 11 are relatively small compared to those of other cases (Cases 2, 14, and 21), the overall combustion proceeds similarly to their corresponding 0-D ignition during the first-stage of ignition; however, for Cases 2, 14, and 21 with relatively large T', the wide span of the first-stage ignition delay in the initial mixture results in the gradual reduction of *n*-heptane and increment of HO_2, which is manifested in the relatively-small and temporally-distributed HRR during the early stage of the ignition (see Figs. 4a and 6 a). In either case, however, the temporal spread of HRR (Cases 2, 4, and 21) during the second-stage ignition is manifested in a gradual increase of OH and decrease of H_2O_2 as the high-temperature chemistry dominates the overall combustion, implying that the overall combustion occurs not only by the spontaneous ignition mode but also by the deflagration mode of combustion.

Second, for cases with T_0 = 933 K (see Fig. 13), only a small fraction of *n*-heptane is rapidly consumed during the first-stage ignition and then, it decreases linearly until the end of combustion. Since the HRR from the first-stage ignition at T_0 = 933 K is much smaller than at T_0 = 805 K, the consumption of *n*-heptane for cases with T_0 = 933 K during the first-stage ignition becomes smaller compared to cases with T_0 = 833 K. For all cases with T_0 = 933 K, HO_2 has two peaks at the first- and second-stage ignition; as discussed above, the first peak occurs through RH + O_2 → R + HO_2 and the second is attributed to the accumulation of HO_2 via R + O_2 → olefin + HO_2 of the intermediate-temperature chemistry. Similar to cases with T_0 = 833 K, the temporal distribution of the mean HRR during the second-stage ignition is manifested in the progressive increment of OH and reduction of

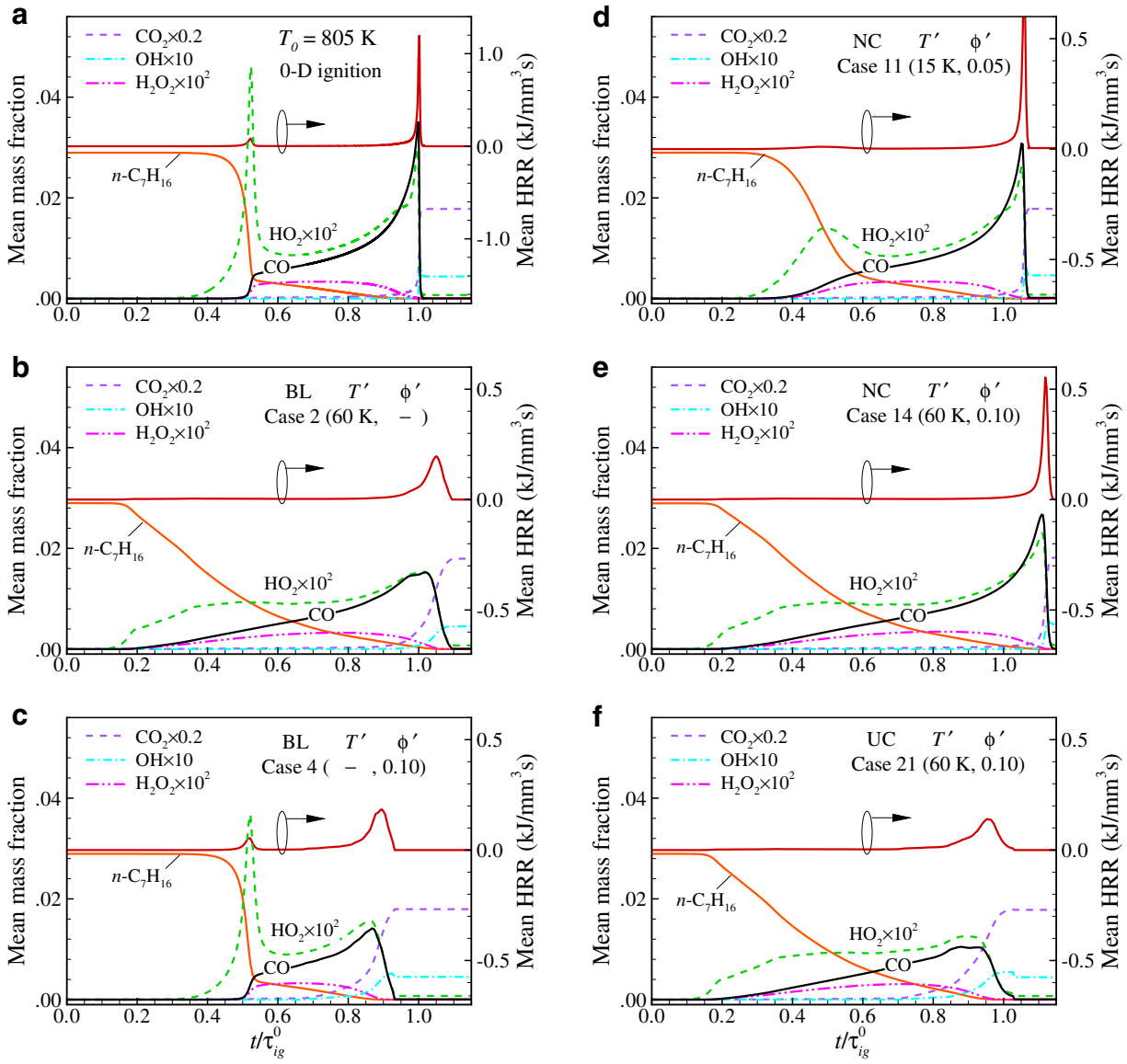

Fig. 12. Temporal evolutions of the mean mass fractions of important species and mean HRR at $T_0 = 805$ K for (a) 0-D ignition, (b) Case 2, (c) Case 7, (d) Case 11, (e) Case 14, and (f) Case 21.

H_2O_2. These results are consistent with the previous DNS study of ignition of primary reference fuel (PRF)/air mixtures of which T_0 lies within the NTC regime [13].

Third, for cases with $T_0 = 1025$ K (see Fig. 14), n-heptane is first gradually consumed and then, the consumption rate keeps increasing till the end of the overall combustion. At high T_0 of 1025 K, there is no first-stage ignition and the intermediate-to-high temperature chemistry govern the ignition such that the consumption of n-heptane and accumulation of HO_2 occurs gradually through the intermediate-temperature chemistry as shown in Fig. 11. As deflagrations developed from ignition kernels propagate into unburnt mixture, significant heat release starts to occur and CO and OH levels increase rapidly. At the final stage, the unburnt mixture is consumed primarily by the spontaneous ignition and as such, the mass fraction of CO and HO_2 decreases rapidly. It is also of interest to note that the level of H_2O_2 concentration is relatively low compared to that at $T_0 =$ 805 and 933 K. At high temperature, H_2O_2 decomposes rapidly into OH via $H_2O_2 + M \rightarrow OH + OH + M$ and as such, remains relatively constant till the thermal ignition.

Overall, the evolution characteristics of important species for 2-D DNS cases are similar to those of the corresponding 0-D ignitions and the departure from the 0-D ignition is primarily attributed to the existence of deflagrations during the combustion, which is controlled by the degree of T' and ϕ' and their spatial correlation.

4.2. Chemical explosive mode analysis

In this section, CEMA is adopted to understand the spatial ignition characteristics of the lean n-heptane/air mixture by identifying controlling species and elementary reactions at different locations and time. CEMA has been applied to various DNS problems such as turbulent lifted jet flames in heated coflows [56,61–63], turbulent reacting jet flames in cross flows [64,65], and ignition of hydrocarbon fuel/air mixtures under HCCI conditions [9,11–13,66]. From these studies, CEMA has been proved as a reliable computational flame diagnostics (CFLD) tool to systematically detect important species and reactions for premixed flames and limit phenomena including ignition and extinction.

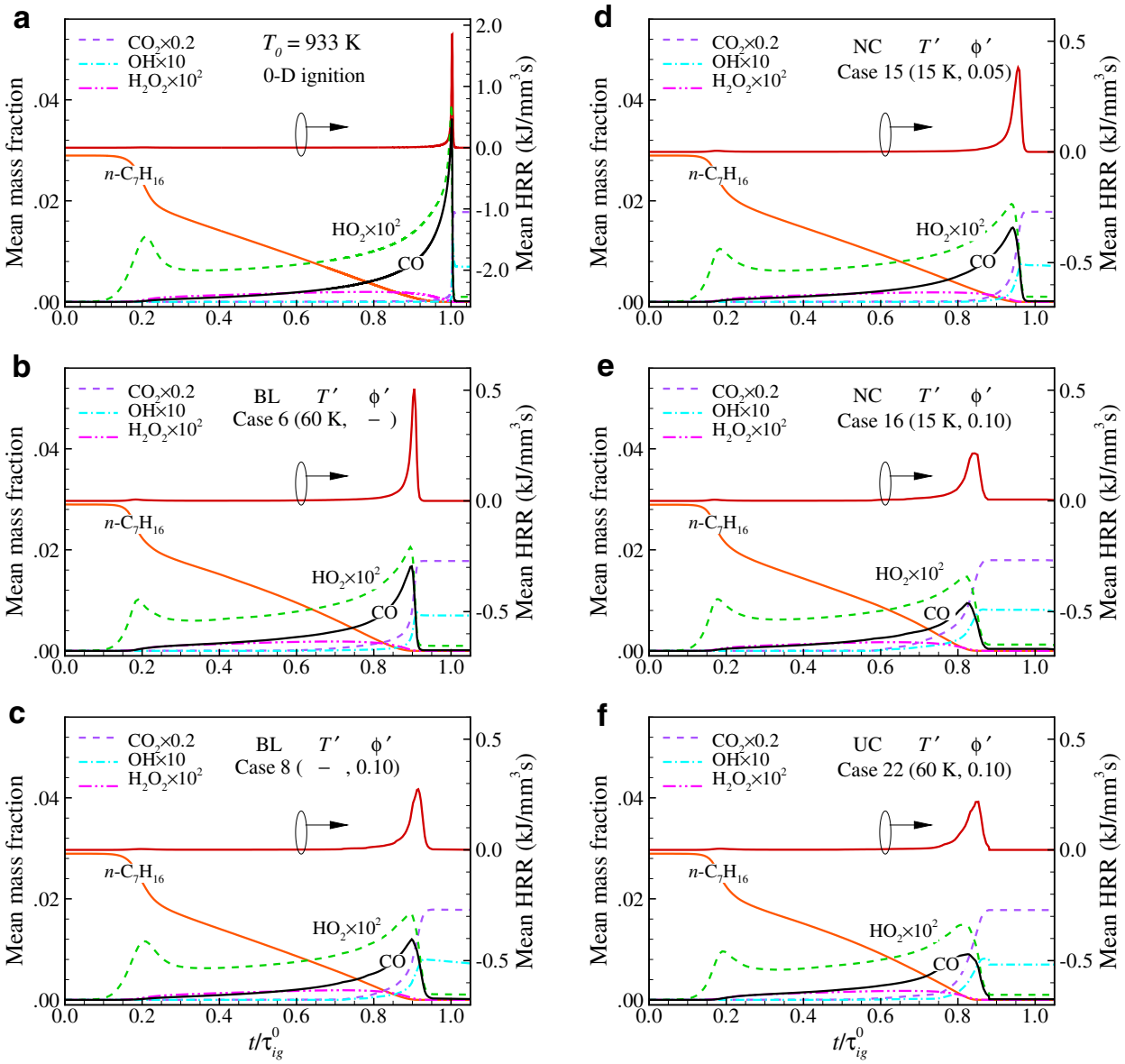

Fig. 13. Temporal evolutions of the mean mass fractions of important species and mean HRR at $T_0 = 933$ K for (a) 0-D ignition, (b) Case 6, (c) Case 8, (d) Case 15, (e) Case 16, and (f) Case 22.

CEMA is briefly explained here and for more details of CEMA, readers are referred to [61,63]. The differential governing equations for a chemically-reacting flow can be described in discretized form as:

$$\frac{D\mathbf{y}}{Dt} = \mathbf{g}(\mathbf{y}) = \boldsymbol{\omega}(\mathbf{y}) + \mathbf{s}(\mathbf{y}), \tag{2}$$

where D/Dt is the material derivative, which can be replaced by d/dt in the Lagrangian coordinate, and $\mathbf{y}$ represents the solution vector of species concentrations and temperature. The chemical source term is denoted as $\boldsymbol{\omega}$, while all non-chemical source terms such as diffusion in flames and homogeneous mixing term in stirred reactors are represented by $\mathbf{s}$.

The Jacobian of the chemical source term, $\mathbf{J}_{\boldsymbol{\omega}}$ ($\equiv \partial\boldsymbol{\omega}/\partial\mathbf{y}$), includes the local chemical information of local mixture and as such, it can be used to determine the chemical feature of the mixture. For this purpose, a chemical mode is defined as an eigenmode of $\mathbf{J}_{\boldsymbol{\omega}}$, which is associated with an eigenvalue, λ_e, and a corresponding pair of the left and right eigenvectors, $\mathbf{b}_e$ and $\mathbf{a}_e$. A chemical explosive mode (CEM) is a chemical mode of which real part of the eigenvalue is positive: $\mathrm{Re}(\lambda_e) > 0$.

The existence of a CEM indicates that the local mixture auto-ignites if there are no thermal and radical losses. In the same way, the auto-ignition of a local mixture exhibiting CEM may be delayed or even fail if the mixture loses significant heat or radicals by strong mixing or diffusion. Nevertheless, CEM remains an intrinsic chemical feature of ignitable mixtures. It is also of interest to note that the critical flame features including ignition, extinction, and premixed flame front locations, are closely related with the transition of CEMs from explosive ($\mathrm{Re}(\lambda_e) > 0$) to non-explosive ($\mathrm{Re}(\lambda_e) < 0$) state as shown in [9,12,13,66].

The competition between the local CEM and mixing loss can be quantitatively measured by a Damköhler number defined as $Da_c = \lambda_e \cdot \chi^{-1}$ [61–63,66]. χ is a scalar dissipation rate defined as $\chi = 2D|\nabla c|^2$, where c and D are a progress variable and the thermal diffusivity of the local mixture, respectively. In the present study, c is evaluated using $c = Y_c/Y_c^{\mathrm{Eq}}$, where $Y_c = Y_{\mathrm{CO}_2} + Y_{\mathrm{CO}}$ and Y_c^{Eq} is the corresponding equilibrium value of Y_c which is found to be 0.09 for the

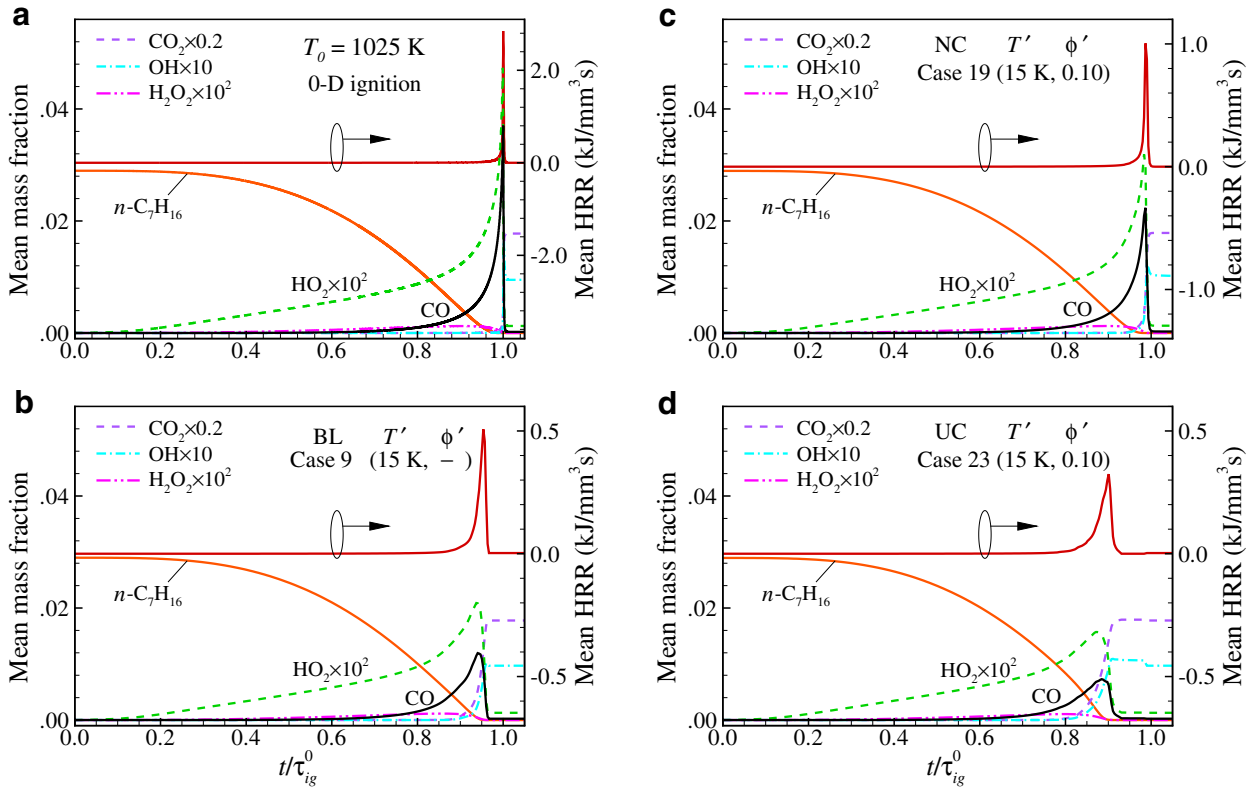

Fig. 14. Temporal evolutions of the mean mass fractions of important species and mean HRR at $T_0 = 1025$ K for (a) 0-D ignition, (b) Case 9, (c) Case 19, and (d) Case 23.

present DNS cases. It should be noted that $Da_c = 1$ is an important criterion for limit phenomena detection. Specifically, at a mixture exhibiting $Da_c = 1$, reaction balances mixing, which occurs usually at the ignition front or flame front; whereas $Da_c \gg 1$ indicates that reaction dominates over diffusion and mixture with $Da_c \gg 1$ will most likely auto-ignite.

The contribution of each variable and reaction to the CEM can be quantified by evaluating the explosive index (EI) of each variable and participation index (PI) of each reaction, which can identify critical chemical kinetic processes during the ignition. The **EI** and **PI** vectors are defined as [63,66]:

$$\mathbf{EI} = \frac{|\mathbf{a}_e \otimes \mathbf{b}_e^T|}{sum(|\mathbf{b}_e \otimes \mathbf{b}_e^T|)}, \tag{3}$$

$$\mathbf{PI} = \frac{|\mathbf{b}_e \cdot \mathbf{S} \otimes \mathbf{R}|}{sum(|(\mathbf{b}_e \cdot \mathbf{S}) \otimes \mathbf{R}|)}, \tag{4}$$

where **S** and **R** represent the stoichiometric coefficient matrix and the vector of the net rates for reactions, respectively and the operator $\otimes$ represents the element-wise multiplication of two vectors. A 88-species skeletal mechanism for *n*-heptane oxidation [9] is used for CEMA to analytically evaluate $\mathbf{J}_{\omega}$, $\mathbf{a}_e$, and $\mathbf{b}_e$.

Figure 15 shows the isocontours of HRR, temperature, *n*-heptane mass fraction, the log-scale of $\mathrm{Re}(\lambda_e)$, and the EI values of important variables which exhibit relatively-large EI values for Case 16 at $t/\tau^0_{ig} = 0.67$. Henceforth, the range of each color legend in figures is determined by the maximum and minimum values of each variable. Two points are to be noted from the figure. First, it is readily observed from Fig. 15a–d that mixture with $\mathrm{Re}(\lambda_e) < 0$ has already ignited while the ignition of mixture with $\mathrm{Re}(\lambda_e) > 0$ is still underway. In between the two distinct regions, there exist thin deflagrations with large HRR and $Da_c \sim O(1)$. Second, temperature, *n*-heptane, and H_2O_2 are the main variables that control the ignition in the unburnt region. More specifically, temperature and *n*-heptane are the main source of the CEM at relatively-low temperature region ($T \sim 1000$ K) while H_2O_2 becomes important for the ignition of unburnt mixture at relatively-high temperature region ($T \sim 1100$ K). This is because fuel decomposition still occurs at the relatively-low temperature region with large fuel concentration. At $T \sim 1100$ K, however, the chain-branching reaction of H_2O_2 becomes highly reactive, which subsequently results in initiating high temperature chemistry.

In addition, CO and OH are found to be the most important species in the burnt region (see Fig. 15h and i) in which the high-temperature chemistry remains controlling the combustion process. It is also found from 1-D profiles of important species and their EI values (not shown here) that from upstream to downstream through deflagrations, EI of CO increases nearly up to unity from zero while EIs of temperature and H_2O_2 vanish rapidly, which is consistent with the characteristics of *n*-heptane oxidation observed in freely-propagating premixed flames and auto-ignition [66].

To further identify critical reactions involving the important species, the isocontours of PI values of important reactions with large PI values are shown in Fig. 16. Note that Fig. 16f shows the cumulative PI value of R293–R300 through which fuel converts into various isomers of alkyl radicals: $\mathrm{RH} + (\mathrm{OH}, \mathrm{HO_2}) \rightarrow \mathrm{R} + (\mathrm{H_2O}, \mathrm{H_2O_2})$. It is generally believed that $\mathrm{CO} + \mathrm{OH} \rightarrow \mathrm{CO_2} + \mathrm{H}$ (R7) and $\mathrm{H} + \mathrm{O_2} \rightarrow \mathrm{O} + \mathrm{OH}$ (R8) are two critical reactions in a hydrocarbon/air combustion process regardless of specific fuel type [60]. In the present study, both reactions are also found to be important to the CEM especially across the deflagrations. This is primarily because R7 is the main conversion path of CO to CO_2 and R8 is the most important chain-branching reaction at high temperature. In addition, HO_2 formation reaction, $\mathrm{H} + \mathrm{O_2} + \mathrm{M} \rightarrow \mathrm{HO_2} + \mathrm{M}$ (R24), is also found to be important at the deflagrations because it is one of the most exothermic reactions in hydrogen/air premixed flames [60].

In the unburnt region upstream of the deflagrations (see Fig. 16e and f), however, it is readily observed that the chain branching of H_2O_2 (R48) and the generation of alkyl radical and H_2O_2

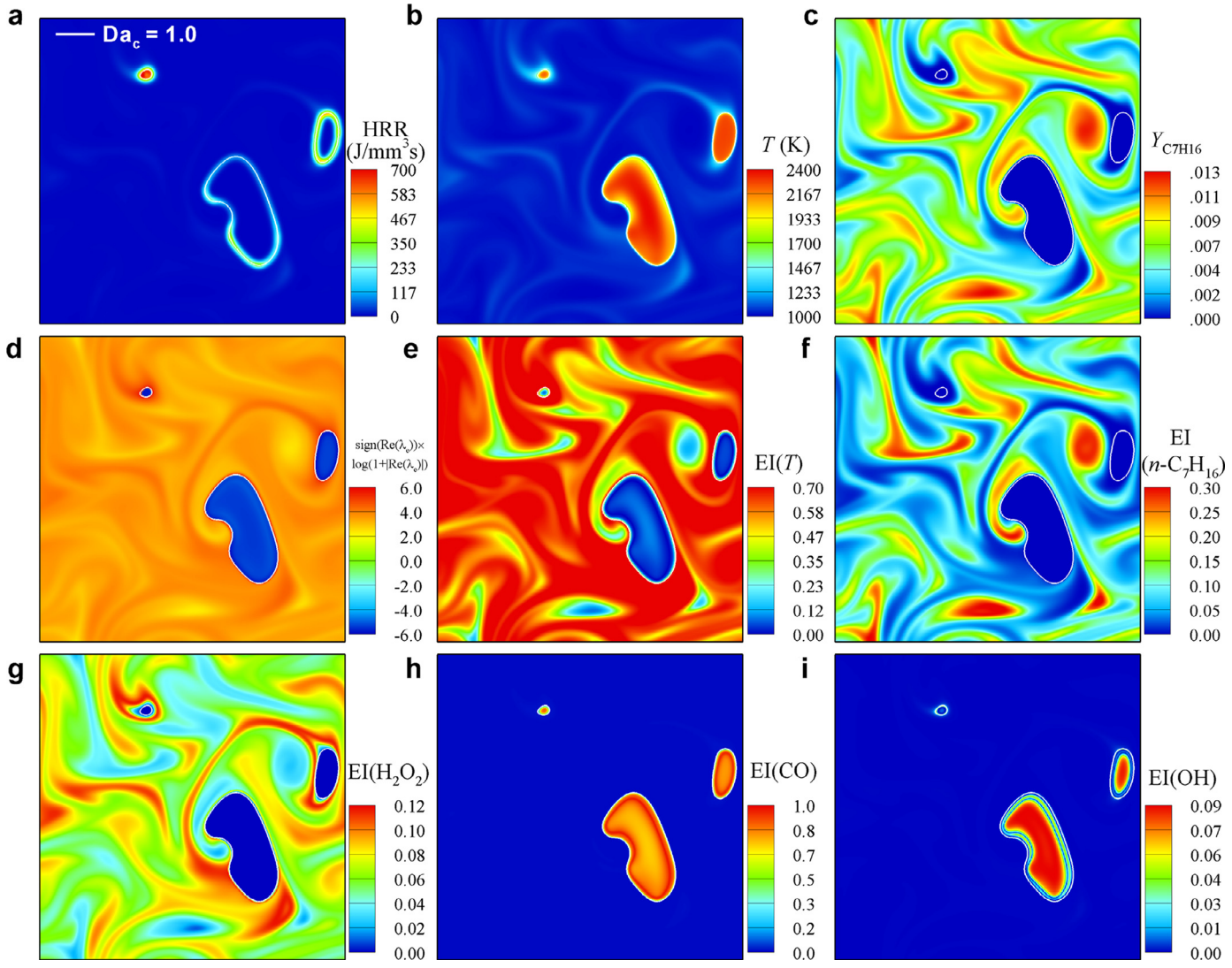

Fig. 15. Isocontours of (a) HRR, (b) temperature, (c) $Y_{C_7H_{16}}$, (d) sign($Re(\lambda_e)$) × log(1+|$Re(\lambda_e)$|), and EI of (e) temperature, (f) *n*-heptane, (g) H_2O_2, (h) CO, and (i) OH for Case 16 (T_0 = 933 K, NC: T' = 15 K and ϕ' = 0.10) at $t/\tau_{ig}^0 = 0.67$. The white solid line represents $Da_c = 1.0$. (For interpretation of the references to color in this figure, the reader is referred to the web version of this article).

(R292–R300) are the most important reactions to the CEM. Consistent with the EI analysis above, the conversion of fuel to alkyl radical and H_2O_2 is important for unburnt mixtures with $T \sim 1000$ K and relatively-high fuel concentration; however, the chain branching reaction of H_2O_2 becomes more important at $T \sim 1100$ K. The result implies that H_2O_2 generated from fuel decomposition reactions becomes reactive at relatively-high temperature region, consequently inducing the thermal ignition of the unburnt mixtures as explained earlier.

The same EI and PI analyses are applied to Case 16 at τ_{ig} (= $0.83\tau_{ig}^0$). Figures 17 and 18 show the isocontours of EI and PI values of the most important species and reactions. Even at the maximum HRR time, thin deflagrations with high HRR and $Da \sim O(1)$ are readily observed with similar characteristics to those of nascent deflagrations at $t = 0.67\tau_{ig}^0$ in terms of EI and PI values. Unlike the ignition characteristics at the early time, however, significant heat is released upstream of the deflagrations by the thermal ignition of unburnt mixtures, which is manifested in large EI values of temperature together with relatively-small EI values of H_2O_2 and non-zero EI values of OH. The occurrence of thermal ignition in the unburnt region is also manifested in relatively-large PI values of high-temperature chain branching reaction (R8) and HO_2 formation/consumption reactions (R24 and R47). Since temperature of the unburnt mixtures is in 1200–1600 K range, the high-temperature chemistry dominates the intermediate-temperature chemistry; the high-temperature chain-branching reaction (R8) becomes more important to the CEM than H_2O_2 decomposition reaction (R49). It is also of interest to note that since *n*-heptane is already decomposed into smaller radicals, it is in low concentration and has little effect on the CEM based on EI and PI values (see Figs. 17c and f, and 18 f).

5. Discussion

In the present study, the effects of turbulence and compression heating on the ignition characteristics of HCCI/SCCI combustion are not investigated not only because it requires too many parametric DNS cases but also because their effects may be expected from previous DNS studies [7–13,36,50].

In general, the overall HCCI combustion with large u' and short τ_t proceeds more similarly to the corresponding 0-D ignition because turbulence with large u' and short τ_t is more apt to homogenize the initial mixture as found in [7–9,11,12]. In the spark-assisted

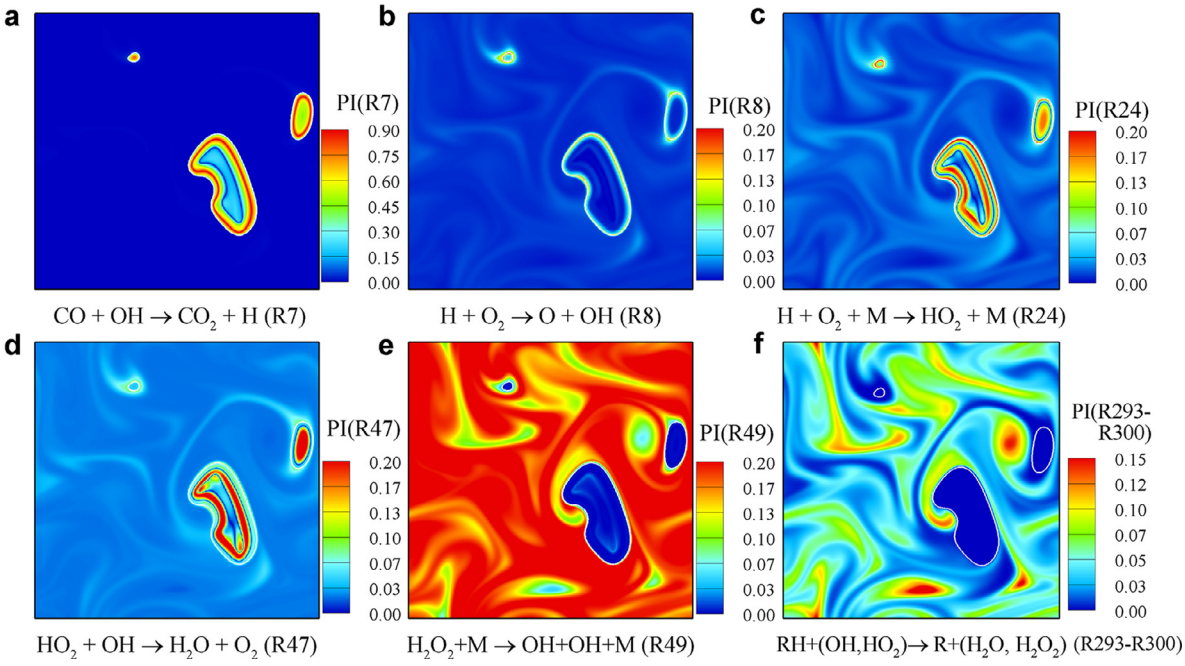

Fig. 16. Isocontours of PIs of controlling reactions for Case 16 ($T_0 = 933$ K, NC: $T' = 15$ K and $\phi' = 0.10$) at $t/\tau_{ig}^0 = 0.67$. The white solid line represents $Da_c = 1.0$.

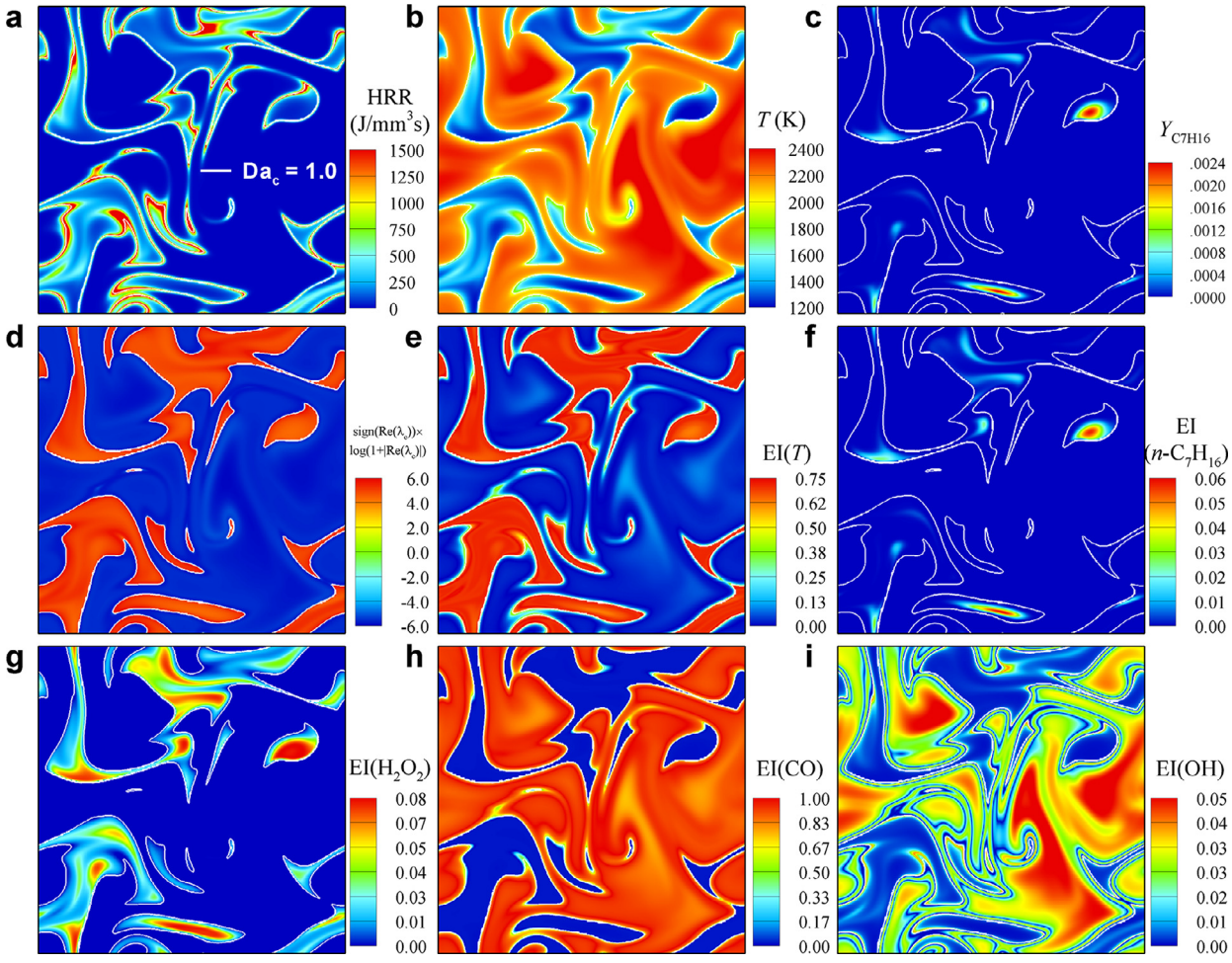

Fig. 17. Isocontours of (a) HRR, (b) temperature, (c) $Y_{C_7H_{16}}$, (d) sign($Re(\lambda_e)$) × log(1+|$Re(\lambda_e)$|), and EI of (e) temperature, (f) n-heptane, (g) H_2O_2, (h) CO, and (i) OH for Case 16 ($T_0 = 933$ K, NC: $T' = 15$ K and $\phi' = 0.10$) at $t/\tau_{ig}^0 = 0.83$. The white solid line represents $Da_c = 1.0$.

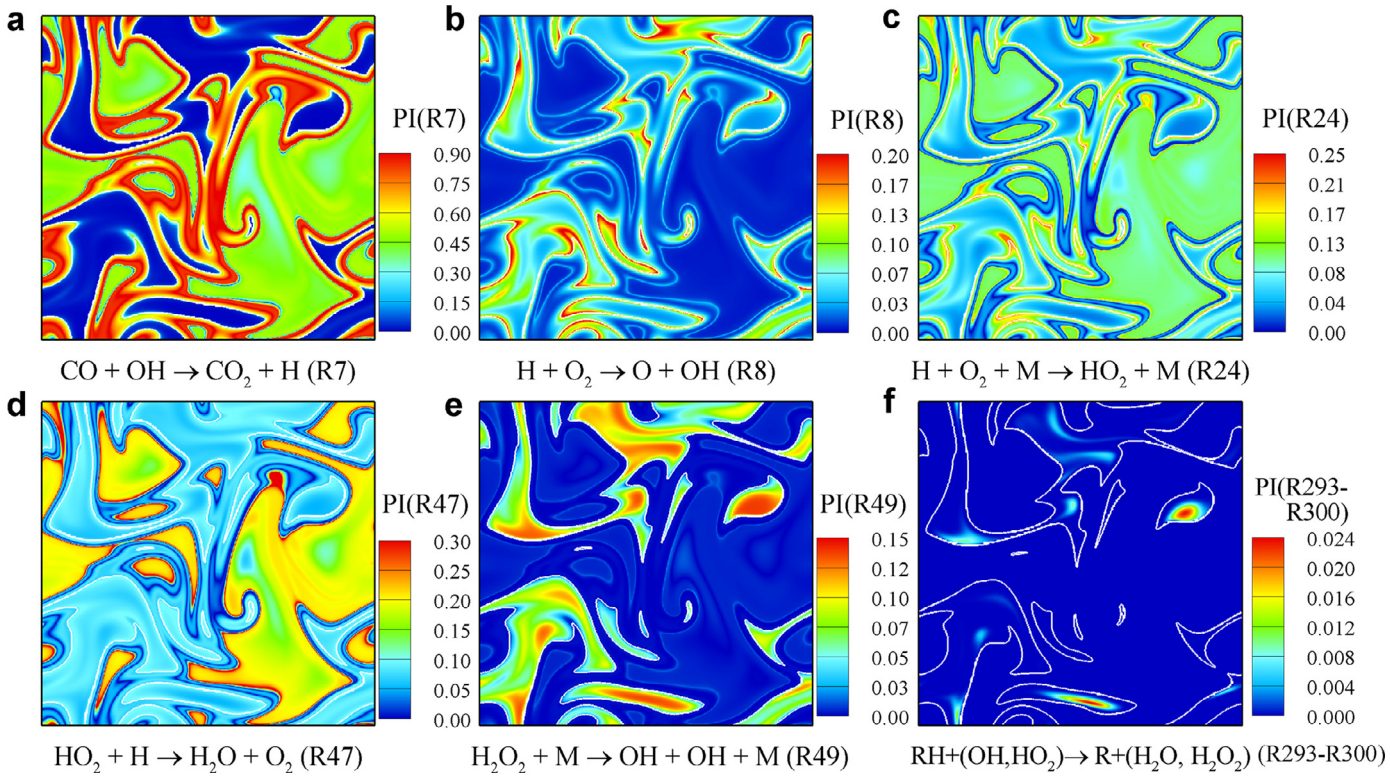

Fig. 18. Isocontours of PIs of controlling reactions for Case 16 ($T_0 = 933$ K, NC: $T' = 15$ K and $\phi' = 0.10$) at $t/\tau_{ig}^0 = 0.83$. The white solid line represents $Da_c = 1.0$.

compression ignition (SACI) combustion [10,36] and HCCI combustion with very large T' [13], however, turbulence with large u' and short τ_t can advance the overall combustion. In both cases, the shortest ignition delay of the initial mixture is much smaller than turbulent mixing timescale such that the evolution of nascent ignition kernels to deflagrations is not affected by the turbulence.

In our previous study [13], the ratio of the shortest ignition delay represented by the lowest 10% ignition delay of initial mixture to turbulent mixing timescale is defined as the ignition Damköhler number, $Da_{ig} \equiv \tau_t/\tau_{ig,10\%}$, such that it exhibits $O(10)$ values in the SACI and HCCI combustion with very large T'. In such cases, once the deflagration waves develop successfully from the ignition kernels, turbulence with large u' tends to enhance turbulent burning rate by increasing turbulent flame area because most HCCI/SACI combustion occur within the corrugated flamelet and thin reaction regimes of the premixed turbulent combustion regime diagram [67,68].

This general description of the effects of turbulent mixing and deflagration on the HCCI combustion can directly be applied to the SCCI combustion. As mentioned earlier, large T' in the HCCI combustion cannot be easily achieved without expensive fuel charge heating and as such, the shorter ignition delay and larger Da_{ig} of initial mixture can be achieved by adopting the fuel stratification in the SCCI combustion. As shown in Fig. 3, the initial ignition delays can be more distributed by the fuel stratification than by the temperature stratification in the intermediate T_0 within the NTC regime. Therefore, turbulent mixing may enhance the overall SCCI combustion if Da_{ig} of the initial mixture is large enough. However, in the SCCI combustion, large ϕ' cannot be expected because local large ϕ can produce more NOx emission and as such, the distribution of local ϕ needs to be strictly below unity as demonstrated in previous experimental studies [24,43]. From this point of view, it may be conjectured that high turbulent mixing generally retards the overall SCCI combustion by homogenizing the initial mixture stratification.

To overcome the disadvantage of the SCCI combustion in developing deflagration waves by reducing the shortest τ_{ig}^0, the concept of reactivity-controlled compression ignition (RCCI) combustion has been devised, in which small τ_{ig}^0 can be achieved by utilizing two different types of fuels: one is high-reactivity fuel such as diesel and the other is low-reactivity fuel such as gasoline. The effect of turbulent mixing and deflagration on the RCCI combustion is an ongoing research topic.

It is also of importance to mention that the combustion phase relative to the TDC can alter the overall HCCI combustion as found in [36,50]. Based on the results in [36,50], it can be conjectured that if combustion occurs near/prior to the TDC, the overall HCCI combustion in the present DNSs can be advanced in time by the compression heating during the compression stroke, featuring in higher peak PRR and shorter burning duration. In experiments, however, the HCCI combustion is designed to occur after the TDC to avoid such excessive PRR under high load conditions. In this situation, the overall HCCI combustion with low T' and/or ϕ' can be further retarded by the expansion effect during the power stroke, resulting in much lower peak PRR and longer burning duration. This expansion effect on HCCI combustion can be more enhanced by the negatively-correlated $T - \phi$ fields in the low temperature regime. On the contrary, large T' and/or ϕ' can still advance the overall HCCI combustion with higher peak PRR and shorter burning duration even if combustion occurs after the TDC. This is because large T' and/or ϕ' can render the overall combustion to occur right after the TDC. These conjectures, however, need to be verified by another set of DNSs.

From the present study, it can be concluded that considering the initial mean temperature and the degree of NTC behavior of given fuel/air mixture, the degree of thermal and compositional stratifications and their correlations need to be carefully chosen to prevent the excessive PRR and determine the ignition timing of HCCI combustion. Furthermore, the present DNS data sets can be utilized to develop and validate several turbulent combustion models for HCCI/SCCI

combustion including flamelet-based models [69], probability density function (PDF)-based models [70], and conditional moment closure (CMC)-based model [71,72] because these models have been reported not to reproduce correctly the results of DNSs of HCCI/SCCI combustion with large T' and/or ϕ' [69–72].

6. Conclusions

The ignition characteristics of thermally- and/or compositionally-stratified lean *n*-heptane/air mixture under HCCI conditions were investigated by performing 2-D DNSs with a 58-species reduced mechanism. From the parametric study, the effects of T', ϕ', and their spatial correlations on the ignition of n-heptane/air mixture were elucidated at three different T_0 of 805, 933, and 1025 K. It was found from the 2-D DNSs:

1. For the BL cases with ϕ' only, the overall combustion occurs more quickly and the mean HRR increases more slowly with increasing ϕ' regardless of T_0.
2. For the BL cases with T' only, the overall combustion is retarded/advanced in time with increasing T' for low/high T_0 relative to the NTC regime resulting from a longer/shorter overall ignition delay of the mixture; for intermediate T_0 within the NTC regime, however, the overall combustion is slightly retarded with small T', while being advanced with large T', exhibiting the combined effects of both low and high T_0 near the NTC regime.
3. For the NC cases, the negative $T-\phi$ correlation has an adverse effect on the overall combustion at low and high T_0: the peak $\bar{\dot{q}}$ is significantly increased while the duration of the main combustion is reduced compared to their corresponding BL cases.
4. For intermediate T_0 within the NTC regime, however, the negatively-correlated $T-\phi$ fields has a synergistic effect on the overall combustion by spreading out $\bar{\dot{q}}$ over time and reducing the peak $\bar{\dot{q}}$.
5. For the UC cases, the mean HRR is more distributed over time and the overall combustion is more advanced in time compared to the corresponding BL cases with T' or ϕ' only except for cases with low T_0.
6. For cases with low T_0, however, the overall combustion is more retarded in time while the mean HRR is more distributed over time compared to the corresponding BL cases with ϕ' only.

These results are primarily attributed to the characteristics of the 0-D ignition delays of initial mixtures such as the shortest τ_{ig}^0 and the span of τ_{ig}^0, which are determined by T', ϕ', and their correlation at different T_0. These results suggest that an appropriate combination of T' and ϕ' together with a well-prepared $T-\phi$ distribution can provide a smooth ignition process and control ignition-timing in HCCI/SCCI combustion.

Chemical explosive mode analysis together with the characteristics of temporal evolution of species identifies important species and reactions for the ignition of *n*-heptane/air mixture at different locations and time. In regions where the spontaneous ignition mode of combustion is predominant, temperature, H_2O_2, and *n*-heptane are identified as the key species for the CEM prior to thermal ignition while the chain branching reaction of H_2O_2 and the conversion reaction of *n*-heptane to alkyl radical and H_2O_2 are the main reactions of the intermediate-temperature chemistry. During thermal ignition, however, temperature is found to be the predominant variable and high-temperature reactions represented by $H + O_2 \rightarrow O + OH$ are responsible for the thermal ignition. At deflagrations, temperature, CO, and OH are found to be the most important variables while the conversion reaction of CO to CO_2 and high-temperature chain branching reaction of $H + O_2 \rightarrow O + OH$ are identified to be important to the CEM.

Acknowledgment

This research was supported by Basic Science Research Program through the National Research Foundation of Korea (NRF) funded by the Ministry of Science, ICT & Future Planning (No. 2015R1A2A2A01007378) and the 2015 Research Fund (1.150033.01) of UNIST. The work at the University of Connecticut was supported by the Chemical Sciences, Geosciences and Biosciences Division, Office of Basic Energy Sciences, Office of Science, US Department of Energy under Grant DE-SC0008622. SHC was supported by Saudi Aramco FUELCOM program through King Abdullah University of Science and Technology (KAUST). This research used the resources of the KAUST Supercomputing Laboratory and UNIST Supercomputing Center.

References

[1] J.E. Dec, Advanced compression-ignition engines–understanding the in-cylinder processes, Proc. Combust. Inst. 32 (2009) 2727–2742.
[2] M. Yao, Z. Zheng, H. Liu, Progress and recent trends in homogeneous charge compression ignition (HCCI) engines, Prog. Energy Combust. Sci. 35 (2009) 398–437.
[3] X. Lü, D. Han, Z. Huang, Fuel design and management for the control of advanced compression-ignition combustion modes, Prog. Energy Combust. Sci. 37 (2011) 741–783.
[4] S. Saxena, I.D. Bedoya, Fundamental phenomena affecting low temperature combustion and HCCI engines, high load limits and strategies for extending these limits, Prog. Energy Combust. Sci. 39 (2013) 457–488.
[5] J.E. Dec, W. Hwang, Characterizing the development of thermal stratification in an HCCI engine using planar-imaging thermometry, SAE Trans. Paper 2009-01-0650 (2009).
[6] R. Sankaran, H.G. Im, E.R. Hawkes, J.H. Chen, The effects of non-uniform temperature distribution on the ignition of a lean homogeneous hydrogen-air mixture, Proc. Combust. Inst. 30 (2005) 875–882.
[7] E.R. Hawkes, R. Sankaran, P. Pébay, J.H. Chen, Direct numerical simulation of ignition front propagation in a constant volume with temperature inhomogeneities: II. parametric study, Combust. Flame 145 (2006) 145–159.
[8] J.H. Chen, E.R. Hawkes, R. Sankaran, S.D. Mason, H.G. Im, Direct numerical simulation of ignition front propagation in a constant volume with temperature inhomogeneities: I. fundamental analysis and diagnostics, Combust. Flame 145 (2006) 128–144.
[9] C.S. Yoo, T. Lu, J.H. Chen, C.K. Law, Direct numerical simulations of ignition of a lean *n*-heptane/air mixture with temperature inhomogeneities at constant volume: Parametric study, Combust. Flame 158 (2011) 1727–1741.
[10] C.. Yoo, Z. Luo, T. Lu, H. Kim, J.H. Chen, A DNS study of ignition characteristics of a lean *iso*-octane/air mixture under HCCI and SACI conditions, Proc. Combust. Inst. 34 (2013) 2985–2993.
[11] M.B. Luong, Z. Luo, T. Lu, S.H. Chung, C.S. Yoo, Direct numerical simulations of the ignition of lean primary reference fuel/air mixtures with temperature inhomogeneities, Combust. Flame 160 (2013) 2038–2047.
[12] M.B. Luong, T. Lu, S.H. Chung, C.S. Yoo, Direct numerical simulations of the ignition of a lean biodiesel/air mixture with temperature and composition inhomogeneities at high pressure and intermediate temperature, Combust. Flame 161 (2014) 2878–2889.
[13] S.O. Kim, M.B. Luong, J.H. Chen, C.S. Yoo, A DNS study of the ignition of lean PRF/air mixtures with temperature inhomogeneities under high pressure and intermediate temperature, Combust. Flame 162 (2015) 717–726.
[14] Y. Yang, J. Dec, N. Dronniou, M. Sjöberg, W. Cannella, Partial fuel stratification to control HCCI heat release rates: fuel composition and other factors affecting pre-ignition reactions of two-stage ignition fuels, SAE Paper 2011-01-1359 (2011).
[15] Y. Yang, J.E. Dec, N. Dronniou, M. Sjöberg, Tailoring HCCI heat-release rates with partial fuel stratification: Comparison of two-stage and single-stage-ignition fuels, Proc. Combust. Inst. 33 (2011) 3047–3055.
[16] M. Sjöberg, J. E.Dec, Smoothing HCCI heat-release rates using partial fuel stratification with two-stage ignition fuels, SAE Trans. Paper 115 (2006) 318–334.
[17] A. Krisman, E.R. Hwakes, S. Kook, M. Sjöberg, J.E. Dec, On the potential of ethanol fuel stratification to extend the high load limit in stratified-charge compression-ignition engines, Fuel 99 (2012) 45–54.
[18] Y. Yang, J. Dec, N. Dronniou, W. Cannella, Boosted HCCI combustion using low-octane gasoline with fully premixed and partially stratified charges, SAE Paper 2012-01-1120 (2012).
[19] R. Yu, X.-S. Bai, Direct numerical simulation of lean hydrogen/air auto-ignition in a constant volume enclosure, Combust. Flame 160 (2013) 1706–1716.
[20] H.A. El-Asrag, Y. Ju, Direct numerical simulations of exhaust gas recirculation effect on multistage autoignition in the negative temperature combustion regime for stratified HCCI flow conditions by using H2O2 addition, Combust. Theory Model. 17 (2013) 316–334.
[21] H.A. El-Asrag, Y. Ju, Direct numerical simulations of NOx effect on multistage autoignition of DME/air mixture in the negative temperature coefficient regime for stratified HCCI engine conditions, Combust. Flame 161 (2014) 256–269.
[22] J.E. Dec, Y. Yang, N. Dronniou, Boosted HCCI-controlling pressure-rise rates for performance improvements using partial fuel stratification with conventional gasoline, SAE Trans. Paper 2011-01-0897 (2011).

[23] J.E. Dec, M. Sjöberg, Isolating the effects of fuel chemistry on combustion phasing in an HCCI engine and the potential of fuel stratification for ignition control, SAE Paper 2004-01-0557 (2004).
[24] W. Hwang, J.E. Dec, M. Sjöberg, Fuel stratification for low-load HCCI combustion: Performance and fuel-PLIF measurements, SAE Trans. Paper 2007-01-4130 116 (2007).
[25] J. Ma, L. Xingcai, L. Ji, Z. Huang, Evaluation of SCCI potentials in comparison to HCCI and conventional DICI combustion using *n*-heptane, Energy Fuels 22 (2008) 954–960.
[26] D. Dahl, M. Andersson, A. Berntsson, I. Denbratt, L. Koopmans, Reducing pressure fluctuations at high loads by means of charge stratification in HCCI combustion with negative valve overlap, SAE Paper 2009-01-1785 (2009).
[27] Y. Wada, J. Senda, Partial fuel stratification to control HCCI heat release rates: Fuel composition and other factors affecting pre-ignition reactions of two-stage ignition fuels, SAE Paper, 2009-01-0498 (2009).
[28] R.E. Herold, J.M. Krasselt, D.E. Foster, J.B. Ghandhi, D.L. Reuss, P.M. Najt, Investigations into the effects of thermal and compositional stratification on HCCI combustion-part II: Optical engine results, SAE Paper 2009-01-1106 (2009).
[29] J. Krasselt, D. Foster, J. Ghandhi, R. Herold, D. Reuss, P. Najt, Investigations into the effects of thermal and compositional stratification on HCCI combustion-part I: Metal engine results, SAE Paper 2009-01-1105 (2009).
[30] G. Bansal, H.G. Im, Autoignition and front propagation in low temperature combustion engine environments, Combust. Flame 158 (2011) 2105–2112.
[31] G. Kalghatgi, L. Hildingsson, A. Harrison, B. Johansson, Autoignition quality of gasoline fuels in partially premixed combustion in diesel engines, Proc. Combust. Inst. 33 (2011) 3015–3021.
[32] A. Viggiano, V. Magi, An investigation on the performance of partially stratified charge CI ethanol engines, SAE Paper 2011-01-0837 (2011).
[33] D. Jung, O. Kwon, O.T. Lim, Comparison of DME HCCI operating ranges for the thermal stratification and fuel stratification based on a multi-zone model, J. Mech. Sci. Technol. 25 (2011) 1383–1390.
[34] V. Mittal, D.J. Cook, H. Pitsch, An extended multi-regime flamelet model for IC engines, Combust. Flame 159 (2012) 2767–2776.
[35] M. Talei, E.R. Hawkes, Ignition in compositionally and thermally stratified *n*-heptane/air mixtures: A direct numerical simulation study, Proc. Combust. Inst. 35 (2015) 3027–3035.
[36] G. Bansal, A. Mascarenhas, J.H. Chen, Direct numerical simulations of autoignition in stratified dimethyl-ether (DME)/air turbulent mixtures, Combust. Flame 162 (2015) 688–702.
[37] R.J. Kee, F.M. Rupley, E. Meeks, J.A. Miller, CHEMKIN-III: A Fortran Chemical Kinetic Package for the Anaylsis of Gas-phase Chemical and Plasma Knietics, Technical Report SAND96-8216, Sandia National Laboratories, 1996.
[38] R.J. Kee, G. Dixon-Lewis, J. Warnatz, M.E. Coltrin, J.A. Miller, A Fortran Computer Code Package for the Evaluation of Gas-phase Multicomponent Transport Properties, Technical Report SAND86-8246, Sandia National Laboratories, 1986.
[39] C.A. Kennedy, M.H. Carpenter, Several new numerical methods for compressible shear-layer simulations, Appl. Num. Math. 14 (1994) 397–433.
[40] C.A. Kennedy, M.H. Carpenter, R.M. Lewis, Low-storage, explicit Runge-Kutta schemes for the compressible Navier-Stokes equations, Appl. Num. Math. 35 (2000) 117–219.
[41] J.H. Chen, A. Choudhary, B. de Supinski, M. DeVries, E.R. Hawkes, S. Klasky, W.K. Liao, K.L. Ma, J. Mellor-Crummey, N. Podhorszki, R. Sankaran, S. Shende, C.S. Yoo, Terascale direct numerical simulations of turbulent combustion using S3D, Comput. Sci. Discov. 2 (2009) 015001.
[42] T. Lu, C.K. Law, C.S. Yoo, J.H. Chen, Dynamic stiffness removal for direct numerical simulations, Combust. Flame 156 (2009) 1542–1551.
[43] S.L. Kokjohn, M.P.B. Musculus, R.D. Reitz, Evaluating temperature and fuel stratification for heat-release rate control in a reactivity-controlled compression-ignition engine using optical diagnostics and chemical kinetics modeling, Combust. Flame 162 (2015) 2729–2742.
[44] A. Hultqvist, M. Christenson, B. Johansson, M. Richter, J. Nygren, J. Hult, M. Alden, The HCCI combustion process in a single cycle-speed fuel tracer LIF and chemiluminescence imaging, SAE Paper 2002-01-0424 (2002).
[45] J.B. Martz, H. Kwak, H.G. Im, G.A. Lavoie, D.N. Assanis, Combustion regime of a reacting front propagating into an auto-igniting mixture, Proc. Combust. Inst. 33 (2011) 1540–7489.
[46] T. Passot, A. Pouquet, Numerical simulation of compressible homogeneous flows in the turbulent regime, J. Fluid Mech. 118 (1987) 441–466.
[47] C.S. Yoo, Y. Wang, A. Trouvé, H.G. Im, Characteristic boundary conditions for direct simulations of turbulent counterflow flames, Combust. Theory Model. 9 (2005) 617–646.
[48] C.S. Yoo, H.G. Im, Characteristic boundary conditions for simulations of compressible reacting flows with multi-dimensional, viscous and reaction effects, Combust. Theory Model. 11 (2007) 259–286.
[49] C.S. Yoo, H.G. Im, Transient soot dynamics in turbulent nonpremixed ethylene-air counterflow flames, Proc. Combust. Inst. 31 (2007) 701–708.
[50] A. Bhagatwala, T. Lu, J.H. Chen, Direct numerical simulations of HCCI/SACI with ethanol, Combust. Flame 161 (2014) 1826–1841.
[51] R. Hasegawa, H. Yanagihara, HCCI combustion in DI diesel engine, SAE Paper 2003-01-0745 (2003).
[52] M. Sjöberg, J.E. Dec, Smoothing HCCI heat-release rates using partial fuel stratification with two-stage ignition fuels, SAE Paper 2006-01-0629 (2006).
[53] J.E. Dec, Y. Yang, Boosted HCCI for high power without engine knock and with ultra-low NOx emissions-using conventional gasoline, SAE Paper 2010-01-1086 (2010).
[54] B. Wolk, J.-Y. Chen, J.E. Dec, Computational study of the pressure dependence of sequential auto-ignition for partial fuel stratification with gasoline, Proc. Combust. Inst. 35 (2015) 2993–3000.
[55] T. Echekki, J.H. Chen, Direct numerical simulation of autoignition in non-homogeneous hydrogen-air mixtures, Combust. Flame 134 (2003) 169–191.
[56] C.S. Yoo, R. Sankaran, J.H. Chen, Three-dimensional direct numerical simulation of a turbulent lifted hydrogen jet flame in heated coflow: flame stabilization and structure, J. Fluid Mech. 640 (2009) 453–481.
[57] H.J. Curran, P. Gaffuri, W.J. Pitz, C.K. Westbrook, A comprehensive modeling study of *n*-heptane oxidation, Combust. Flame 114 (1998) 149–177.
[58] H.J. Curran, P. Gaffuri, W.J. Pitz, C.K. Westbrook, A comprehensive modeling study of *iso*-octane oxidation, Combust. Flame 129 (2002) 253–280.
[59] S. Tanaka, F. Ayala, J.C. Keck, J.B. Heywood, Two-stage ignition in HCCI combustion and HCCI control by fuels and additives, Combust. Flame 132 (2003) 219–239.
[60] C.K. Law, Combustion Physics, Combustion Physics, Cambridge University Press, 2006.
[61] T. Lu, C.S. Yoo, J.H. Chen, C.K. Law, Three-dimensional direct numerical simulation of a turbulent lifted hydrogen jet flame in heated coflow: a chemical explosive mode analysis, J. Fluid Mech. 652 (2010) 45–64.
[62] C.S. Yoo, E.S. Richardson, R. Sankaran, J.H. Chen, A DNS study on the stabilization mechanism of a turbulent lifted ethylene jet flame in highly-heated coflow, Proc. Combust. Inst. 33 (2011) 1619–1627.
[63] Z. Luo, C.S. Yoo, E.S. Richardson, J.H. Chen, C.K. Law, T. Lu, Chemical explosive mode analysis for a turbulent lifted ethylene jet flame in highly-heated coflow, Combust. Flame 159 (2012) 265–274.
[64] R.W. Grout, A. Gruber, C.S. Yoo, J.H. Chen, Direct numerical simulation of flame stabilization downstream of a transverse fuel jet in cross-flow, Proc. Combust. Inst. 33 (2011) 1629–1637.
[65] H. Kolla, R.W. Grout, A. Gruber, J.H. Chen, Mechanisms of flame stabilization and blowout in a reacting turbulent hydrogen jet in cross-flow, Combust. Flame 159 (2012) 2755–2766.
[66] R. Shan, C.S. Yoo, J.H. Chen, T. Lu, Computational diagnostics for *n*-heptane flames with chemical explosive mode analysis, Combust. Flame 159 (2012) 3119–3127.
[67] R. Borghi, Turbulent combustion modelling, Prog. Energy Combust. Sci. 14 (1988) 245–292.
[68] N. Peters, Turbulent combustion, Cambridge University Press, 2000.
[69] D.J. Cook, H. Pitch, J.H. Chen, E.R. Hawkes, Flamelet-based modeling of auto-ignition with thermal inhomogeneities for application to HCCI engines, Proc. Combust. Inst. 31 (2007) 2903–2911.
[70] F. Bisetti, J.-Y. Chen, J.H. Chen, E.R. Hawkes, Probability density function treatment of turbulence/chemistry inter-actions during the ignition of a temperature-stratified mixture for application to HCCI engine modeling, Combust. Flame 155 (2008) 571–584.
[71] F. Salehi, M. Talei, E.R. Hawkes, C.S. Yoo, T. Lucchini, G. D'Errico, S. Kook, Conditional moment closure modelling for HCCI with temperature inhomogeneities, Proc. Combust. Inst. 35 (2015) 3087–3095.
[72] F. Salehi, M. Talei, E.R. Hawkes, C.S. Yoo, T. Lucchini, G. D'Errico, S. Kook, A comparative study of conditional moment closure modelling for ignition of *iso*-octane and *n*-heptane in thermally stratified mixtures, Flow Turbul. Combust. 95 (2015) 1–28.